A&A 674, A36 (2023)
https://doi.org/10.1051/0004-6361/202243767
© The Authors 2023

Astronomy & Astrophysics
Special issue

Gaia Data Release 3

Gaia Data Release 3

Pulsations in main sequence OBAF-type stars

Gaia Collaboration: J. De Ridder[1,⋆], V. Ripepi[2], C. Aerts[1,3,4], L. Palaversa[5,6], L. Eyer[7], B. Holl[7,8], M. Audard[7,8], L. Rimoldini[8], A. G. A. Brown[9], A. Vallenari[10], T. Prusti[11], J. H. J. de Bruijne[11], F. Arenou[12], C. Babusiaux[13,12], M. Biermann[14], O. L. Creevey[15], C. Ducourant[16], D. W. Evans[6], R. Guerra[17], A. Hutton[18], C. Jordi[19], S. A. Klioner[20], U. L. Lammers[17], L. Lindegren[21], X. Luri[19], F. Mignard[15], C. Panem[22], D. Pourbaix[23,24,†], S. Randich[25], P. Sartoretti[12], C. Soubiran[16], P. Tanga[15], N. A. Walton[6], C. A. L. Bailer-Jones[4], U. Bastian[14], R. Drimmel[26], F. Jansen[27,⋆⋆], D. Katz[12], M. G. Lattanzi[26,28], F. van Leeuwen[6], J. Bakker[17], C. Cacciari[29], J. Castañeda[30], F. De Angeli[6], C. Fabricius[19], M. Fouesneau[4], Y. Frémat[31], L. Galluccio[15], A. Guerrier[22], U. Heiter[32], E. Masana[19], R. Messineo[33], N. Mowlavi[7], C. Nicolas[22], K. Nienartowicz[34,8], F. Pailler[22], P. Panuzzo[12], F. Riclet[22], W. Roux[22], G. M. Seabroke[35], R. Sordo[10], F. Thévenin[15], G. Gracia-Abril[36,14], J. Portell[19], D. Teyssier[37], M. Altmann[14,38], R. Andrae[4], I. Bellas-Velidis[39], K. Benson[35], J. Berthier[40], R. Blomme[31], P. W. Burgess[6], D. Busonero[26], G. Busso[6], H. Cánovas[37], B. Carry[15], A. Cellino[26], N. Cheek[41], G. Clementini[29], Y. Damerdji[42,43], M. Davidson[44], P. de Teodoro[17], M. Nuñez Campos[18], L. Delchambre[42], A. Dell'Oro[25], P. Esquej[45], J. Fernández-Hernández[46], E. Fraile[45], D. Garabato[47], P. García-Lario[17], E. Gosset[42,24], R. Haigron[12], J.-L. Halbwachs[48], N. C. Hambly[44], D. L. Harrison[6,49], J. Hernández[17], D. Hestroffer[40], T. Hilger[20], S. T. Hodgkin[6], K. Janßen[50], G. Jevardat de Fombelle[7], S. Jordan[14], A. Krone-Martins[51,52], A. C. Lanzafame[53,54], W. Löffler[14], O. Marchal[48], P. M. Marrese[55,56], A. Moitinho[51], K. Muinonen[57,58], P. Osborne[6], E. Pancino[25,56], T. Pauwels[31], A. Recio-Blanco[15], C. Reylé[59], M. Riello[6], T. Roegiers[60], J. Rybizki[4], L. M. Sarro[61], C. Siopis[23], M. Smith[35], A. Sozzetti[26], E. Utrilla[18], M. van Leeuwen[6], U. Abbas[26], P. Ábrahám[62,63], A. Abreu Aramburu[46], J. J. Aguado[61], M. Ajaj[12], F. Aldea-Montero[17], G. Altavilla[55,56], M. A. Álvarez[47], J. Alves[64], F. Anders[19], R. I. Anderson[65], E. Anglada Varela[46], T. Antoja[19], D. Baines[37], S. G. Baker[35], L. Balaguer-Núñez[19], E. Balbinot[66], Z. Balog[14,4], C. Barache[38], D. Barbato[7,26], M. Barros[51], M. A. Barstow[67], S. Bartolomé[19], J.-L. Bassilana[68], N. Bauchet[12], U. Becciani[53], M. Bellazzini[29], A. Berihuete[69], M. Bernet[19], S. Bertone[70,71,26], L. Bianchi[72], A. Binnenfeld[73], S. Blanco-Cuaresma[74], T. Boch[48], A. Bombrun[75], D. Bossini[76], S. Bouquillon[38,77], A. Bragaglia[29], L. Bramante[33], E. Breedt[6], A. Bressan[78], N. Brouillet[16], E. Brugaletta[53], B. Bucciarelli[26,28], A. Burlacu[79], A. G. Butkevich[26], R. Buzzi[26], E. Caffau[12], R. Cancelliere[80], T. Cantat-Gaudin[19,4], R. Carballo[81], T. Carlucci[38], M. I. Carnerero[26], J. M. Carrasco[19], L. Casamiquela[16,12], M. Castellani[55], A. Castro-Ginard[9], L. Chaoul[22], P. Charlot[16], L. Chemin[82], V. Chiaramida[33], A. Chiavassa[15], N. Chornay[6], G. Comoretto[37,83], G. Contursi[15], W. J. Cooper[84,26], T. Cornez[68], S. Cowell[6], F. Crifo[12], M. Cropper[35], M. Crosta[26,85], C. Crowley[75], C. Dafonte[47], A. Dapergolas[39], P. David[40], P. de Laverny[15], F. De Luise[86], R. De March[33], R. de Souza[87], A. de Torres[75], E. F. del Peloso[14], E. del Pozo[18], M. Delbo[15], A. Delgado[45], J.-B. Delisle[7], C. Demouchy[88], T. E. Dharmawardena[4], S. Diakite[89], C. Diener[6], E. Distefano[53], C. Dolding[35], H. Enke[50], C. Fabre[90], M. Fabrizio[55,56], S. Faigler[91], G. Fedorets[57,92], P. Fernique[48,93], F. Figueras[19], Y. Fournier[50], C. Fouron[79], F. Fragkoudi[94,95,96], M. Gai[26], A. Garcia-Gutierrez[19], M. Garcia-Reinaldos[17], M. García-Torres[97], A. Garofalo[29], A. Gavel[32], P. Gavras[45], E. Gerlach[20], R. Geyer[20], P. Giacobbe[26], G. Gilmore[6], S. Girona[98], G. Giuffrida[55], R. Gomel[91], A. Gomez[47], J. González-Núñez[41,99], I. González-Santamaría[47], J. J. González-Vidal[19], M. Granvik[57,100], P. Guillout[48], J. Guiraud[22], R. Gutiérrez-Sánchez[37], L. P. Guy[8,101], D. Hatzidimitriou[102,39], M. Hauser[4,103], M. Haywood[12], A. Helmer[68], A. Helmi[66], M. H. Sarmiento[18], S. L. Hidalgo[104,105], N. Hładczuk[17,106], D. Hobbs[21], G. Holland[6], H. E. Huckle[35], K. Jardine[107], G. Jasniewicz[108], A. Jean-Antoine Piccolo[22], Ó. Jiménez-Arranz[19], J. Juaristi Campillo[14], F. Julbe[19], L. Karbevska[8,109], P. Kervella[110], S. Khanna[66,26], G. Kordopatis[15], A. J. Korn[32], Á Kóspál[62,4,63], Z. Kostrzewa-Rutkowska[9,111], K. Kruszyńska[112], M. Kun[62], P. Laizeau[113], S. Lambert[38], A. F. Lanza[53], Y. Lasne[68], J.-F. Le Campion[16], Y. Lebreton[110,114], T. Lebzelter[64], S. Leccia[2], N. Leclerc[12], I. Lecoeur-Taibi[8], S. Liao[115,26,116], E. L. Licata[26], H. E. P. Lindstrøm[26,117,118], T. A. Lister[119], E. Livanou[102], A. Lobel[31], A. Lorca[18], C. Loup[48], P. Madrero Pardo[19], A. Magdaleno Romeo[79], S. Managau[68], R. G. Mann[44], M. Manteiga[120], J. M. Marchant[121], M. Marconi[2], J. Marcos[37], M. M. S. Marcos Santos[41], D. Marín Pina[19],

⋆ Corresponding author: J. De Ridder, e-mail: joris.deridder@kuleuven.be
⋆⋆ Retired.

Open Access article, published by EDP Sciences, under the terms of the Creative Commons Attribution License (https://creativecommons.org/licenses/by/4.0), which permits unrestricted use, distribution, and reproduction in any medium, provided the original work is properly cited.
This article is published in open access under the Subscribe to Open model. Subscribe to A&A to support open access publication.

S. Marinoni[55,56], F. Marocco[122], D. J. Marshall[123], L. Martin Polo[41], J. M. Martín-Fleitas[18], G. Marton[62], N. Mary[68], A. Masip[19], D. Massari[29], A. Mastrobuono-Battisti[12], T. Mazeh[91], P. J. McMillan[21], S. Messina[53], D. Michalik[11], N. R. Millar[6], A. Mints[50], D. Molina[19], R. Molinaro[2], L. Molnár[62,124,63], G. Monari[48], M. Monguió[19], P. Montegriffo[29], A. Montero[18], R. Mor[19], A. Mora[18], R. Morbidelli[26], T. Morel[42], D. Morris[44], T. Muraveva[29], C. P. Murphy[17], I. Musella[2], Z. Nagy[62], L. Noval[68], F. Ocaña[37,125], A. Ogden[6], C. Ordenovic[15], J. O. Osinde[45], C. Pagani[67], I. Pagano[53], P. A. Palicio[15], L. Pallas-Quintela[47], A. Panahi[91], S. Payne-Wardenaar[14], X. Peñalosa Esteller[19], A. Penttilä[57], B. Pichon[15], A. M. Piersimoni[86], F.-X. Pineau[48], E. Plachy[62,124,63], G. Plum[12], E. Poggio[15,26], A. Prša[126], L. Pulone[55], E. Racero[41,125], S. Ragaini[29], M. Rainer[25,127], C. M. Raiteri[26], P. Ramos[19,48], M. Ramos-Lerate[37], P. Re Fiorentin[26], S. Regibo[1], P. J. Richards[128], C. Rios Diaz[45], A. Riva[26], H.-W. Rix[4], G. Rixon[6], N. Robichon[12], A. C. Robin[59], C. Robin[68], M. Roelens[7], H. R. O. Rogues[88], L. Rohrbasser[8], M. Romero-Gómez[19], N. Rowell[44], F. Royer[12], D. Ruz Mieres[6], K. A. Rybicki[112], G. Sadowski[23], A. Sáez Núñez[19], A. Sagristà Sellés[14], J. Sahlmann[45], E. Salguero[46], N. Samaras[31,129], V. Sanchez Gimenez[19], N. Sanna[25], R. Santoveña[47], M. Sarasso[26], M. Schultheis[15], E. Sciacca[53], M. Segol[88], J. C. Segovia[41], D. Ségransan[7], D. Semeux[90], S. Shahaf[130], H. I. Siddiqui[131], A. Siebert[48,93], L. Siltala[57], A. Silvelo[47], E. Slezak[15], I. Slezak[15], R. L. Smart[26], O. N. Snaith[12], E. Solano[132], F. Solitro[33], D. Souami[110,133], J. Souchay[38], A. Spagna[26], L. Spina[10], F. Spoto[74], I. A. Steele[121], H. Steidelmüller[20], C. A. Stephenson[37,134], M. Süveges[135], J. Surdej[42,136], L. Szabados[62], E. Szegedi-Elek[62], F. Taris[38], M. B. Taylor[137], R. Teixeira[87], L. Tolomei[33], N. Tonello[98], F. Torra[30], J. Torra[19,†], G. Torralba Elipe[47], M. Trabucchi[138,7], A. T. Tsounis[139], C. Turon[12], A. Ulla[140], N. Unger[7], M. V. Vaillant[68], E. vanDillen[88], W. van Reeven[141], O. Vanel[12], A. Vecchiato[26], Y. Viala[12], D. Vicente[98], S. Voutsinas[44], M. Weiler[19], T. Wevers[6,142], Ł. Wyrzykowski[112], A. Yoldas[6], P. Yvard[88], H. Zhao[15], J. Zorec[143], S. Zucker[73], T. Zwitter[144]

(Affiliations can be found after the references)

Received 12 April 2022 / Accepted 24 May 2022

ABSTRACT

Context. The third *Gaia* data release provides photometric time series covering 34 months for about 10 million stars. For many of those stars, a characterisation in Fourier space and their variability classification are also provided. This paper focuses on intermediate- to high-mass (IHM) main sequence pulsators ($M \geq 1.3\,M_{\odot}$) of spectral types O, B, A, or F, known as β Cep, slowly pulsating B (SPB), δ Sct, and γ Dor stars. These stars are often multi-periodic and display low amplitudes, making them challenging targets to analyse with sparse time series.

Aims. We investigate the extent to which the sparse *Gaia* DR3 data can be used to detect OBAF-type pulsators and discriminate them from other types of variables. We aim to probe the empirical instability strips and compare them with theoretical predictions. The most populated variability class is that of the δ Sct variables. For these stars, we aim to confirm their empirical period-luminosity (PL) relation, and verify the relation between their oscillation amplitude and rotation.

Methods. All datasets used in this analysis are part of the *Gaia* DR3 data release. The photometric time series were used to perform a Fourier analysis, while the global astrophysical parameters necessary for the empirical instability strips were taken from the *Gaia* DR3 `gspphot` tables, and the $v \sin i$ data were taken from the *Gaia* DR3 `esphs` tables. The δ Sct PL relation was derived using the same photometric parallax method as the one recently used to establish the PL relation for classical Cepheids using *Gaia* data.

Results. We show that for nearby OBAF-type pulsators, the *Gaia* DR3 data are precise and accurate enough to pinpoint them in the Hertzsprung-Russell (HR) diagram. We find empirical instability strips covering broader regions than theoretically predicted. In particular, our study reveals the presence of fast rotating gravity-mode pulsators outside the strips, as well as the co-existence of rotationally modulated variables inside the strips as reported before in the literature. We derive an extensive period–luminosity relation for δ Sct stars and provide evidence that the relation features different regimes depending on the oscillation period. We demonstrate how stellar rotation attenuates the amplitude of the dominant oscillation mode of δ Sct stars.

Conclusions. The *Gaia* DR3 time-series photometry already allows for the detection of the dominant (non-)radial oscillation mode in about 100 000 intermediate- and high-mass dwarfs across the entire sky. This detection capability will increase as the time series becomes longer, allowing the additional delivery of frequencies and amplitudes of secondary pulsation modes.

Key words. asteroseismology – stars: rotation – stars: oscillations – stars: early-type

1. Introduction

Intermediate- and high-mass (IHM) main sequence stars ($M \geq 1.3\,M_{\odot}$, spectral types O, B, A, and F) have convective cores whose physical conditions cannot be extrapolated from dwarf stars like our Sun. The transport processes caused by internal convection, rotation, and magnetism in IHM dwarfs are far less understood than those in Sun-like stars, yet these processes have a large impact on their evolution and their age determination. A large fraction of the IHM stars are oscillators located in the β Cep, slowly pulsating B (SPB), δ Sct, or γ Dor instability strips in the Hertzsprung-Russell (HR) diagram. β Cep, SPB, and δ Sct stars all exhibit self-excited oscillation modes caused by the conversion of thermal energy into mechanical energy by the so-called κ-mechanism (Pamyatnykh 1999). γ Dor oscillations are driven by a combination of the κ-mechanism on one hand, and radiative flux modulation caused by convection at the bottom of the convective envelope on the other hand. The first mechanism plays a more important role for the hotter γ Dor stars, while the second one is predominant for the cooler γ Dor stars (Guzik et al. 2000; Dupret et al. 2005; Xiong et al. 2016). For all four types of these pulsators, asteroseismology is a particularly promising tool to investigate their internal physics (e.g., Aerts 2021).

† Deceased.

Space telescopes like CoRoT (Auvergne et al. 2009), *Kepler* (Koch et al. 2010), and TESS (Ricker et al. 2016) were dedicated to the gathering of long uninterrupted high-cadence photometry with μmag precision. This type of photometric light curve assembled from space brought unprecedented capabilities to test and calibrate the theory of stellar structure for stars of various masses and evolutionary stages (see Hekker & Christensen-Dalsgaard 2017; García & Ballot 2019; Kurtz 2023, for extensive observational reviews). Thanks to these high-quality data, the high-dimensional problem of asteroseismic modelling of IHM stars becomes achievable (Aerts et al. 2018). Asteroseismic modelling requires identification of the pulsation modes in terms of their spherical wave numbers (ℓ, m) and radial order n. Compared to the simple case of Sun-like stars, the Coriolis force as well as the non-linear interplay between rotation, convection, and magnetism adds a high level of complexity to the modelling of β Cep, SPB, γ Dor, and δ Sct stars. This is why detailed asteroseismic modelling has so far only been carried out for a few tens of such IHM dwarfs, and with inhomogeneous approaches and levels of detail (Degroote et al. 2010; Kurtz et al. 2014; Saio et al. 2015; Murphy et al. 2016; Schmid & Aerts 2016; Deng et al. 2018; Szewczuk & Daszyńska-Daszkiewicz 2018; Mombarg et al. 2019, 2020, 2021; Wu et al. 2020; Pedersen et al. 2021; Sekaran et al. 2021).

In this paper, we present a performance verification of *Gaia* DR3 in terms of the mission's capacity to detect radial and non-radial oscillations of oscillating IHM stars on the main sequence. The *Gaia* space mission was primarily designed as an astrometric mission to reach μas precision. To reach this goal, the CCD detections of the sources do not need to have a very high signal-to-noise ratio (S/N) per field of view transit, nor does the sampling need to be dense.

As a result, *Gaia* photometric time series of an individual star were not meant to be particularly attractive for asteroseismology. The median number of measurements per star is only around 50 in *Gaia* DR3 and their time sampling is sparse. The photometric precision in the G passband is of the order of a mmag. This compares excellently with ground-based surveys, but is not (and never was intended to be) able to compete with the photometric precision of dedicated space missions like *Kepler* or TESS (cf. Appendix A). However, the main advantage of the *Gaia* mission for asteroseismology is the sheer number of sources for which it gathers data. Unlike the *Kepler* or TESS space missions focusing on a relatively small part of the sky or only on brighter stars, respectively, *Gaia* is an all-sky survey covering stars spanning more than 12 orders of magnitude in brightness. In addition, its high angular resolution allows us to also probe the denser parts of the sky. Therefore, *Gaia* enables the detection of oscillations in a far larger number of variable stars. *Gaia* already proved to be an excellent instrument to detect radially oscillating high-amplitude variables (e.g., Clementini et al. 2019; Mowlavi et al. 2018; Ripepi et al. 2022; Gaia Collaboration 2019), but its capacity has not yet been established for the low-amplitude main sequence IHM stars. While the μmag-precision space missions so far resulted in asteroseismic modelling of thousands of red giants (Hon et al. 2018; Yu et al. 2018, 2020, 2021; Stello et al. 2022) and of hundreds of Sun-like dwarfs with masses $M \leq 1.3\,M_\odot$ (García & Ballot 2019), the samples of asteroseismically modelled IHM dwarfs are much smaller and do not yet fully cover the parameter space in terms of rotation, binarity, and metallicity. It is in this area that *Gaia*'s time series is helpful and will allow for the discovery of thousands of oscillating IHM candidates, with the aim being to achieve unbiased and complete samples. These will then become suitable for ensemble asteroseismology in the future, once dedicated high-cadence high-precision monitoring for their members has become available.

In terms of impact, *Gaia* DR3 (and later data releases) may lead to the discovery of tens of thousands of new IHM pulsating dwarfs, delivering the frequencies and amplitudes of their dominant (non)radial oscillation mode(s), aside from a high-precision parallax. Here, we assess *Gaia*'s performance on this front, offering as well an observational census of the instability strips along the upper main sequence for samples of new pulsating IHM dwarfs with $M \geq 1.3\,M_\odot$. The borders of those instability strips depend on the physics of internal rotation, gravitational settling, radiative levitation, shear mixing, and so on, as well as on the bulk metallicity and possible binarity at birth. Given the complex (often non-linear) interplay of these astrophysical phenomena during the evolution and the initial conditions at birth, samples of thousands of (non-)radial pulsators are required to interpret the borders of the instability strips in terms of the excitation physics (Townsend 2005; Szewczuk & Daszyńska-Daszkiewicz 2017) and transport processes (Aerts et al. 2019).

This paper is one among several publications led by the *Gaia* Data Processing Analysis Consortium (DPAC) accompanying the *Gaia* DR3. We present the *Gaia* photometric dataset of variable IHM dwarfs in Sect. 2 and develop our strategies to detect IHM main sequence pulsators in Sect. 3, distinguishing non-radial gravity-mode (g mode) pulsators from (non-)radial pressure-mode (p mode) pulsators. We compare the samples of IHM dwarf pulsators with those in the literature in Sect. 4 and move on to *Gaia*'s performance in Sect. 5, highlighting some dedicated applications. We conclude in Sect. 6 with an explicit encouragement and invitation to the worldwide astrophysics community to exhaustively exploit the *Gaia* time-series data in its full glory.

2. The dataset

Within the *Gaia* Data Processing and Analysis Consortium (DPAC), the CU7 coordination unit responsible for analysing variable stars processed a grand total of 1 840 651 642 sources, of which 25% of the most variable sources were selected for further investigation. This variability was tested in the time domain rather than the Fourier domain for computational reasons, as described in Eyer et al. (2023). These variable sources were then further characterised in the Fourier domain and classified by multiple classifiers each with their own setup Rimoldini et al. (2023). We also refer to the documentation provided by Rimoldini (2022) for further processing details.

For this paper, we started with those 450 605 variable sources from the *Gaia* DR3 table `vari_classifier_result` with at least 40 photometric measurements in the *Gaia* G-band, and which the CU7 classification team classified as either β Cep, δ Sct, SX Phe, SPB, or γ Dor star. No constraints were put on the apparent G magnitude. To this sample we added the 54 476 IHM main sequence pulsator candidates from the *Gaia* DR3 table `vari_ms_oscillator` in *Gaia* DR3, which used a different set of classification criteria. We filtered out any duplicates common to both samples to end up with a sample of 460 519 candidate main sequence variables with at least 40 *Gaia* G data points. Both classifications mentioned here are based on a list of attributes that includes the main frequency ν_1 found in the generalised Lomb-Scargle periodogram (Zechmeister & Kürster 2009). This main frequency optimises the fit of the following

model to the data:

$$G_n = C + A\sin(2\pi\nu_1 t_n + \varphi), \quad (1)$$

where G_n is the observed *Gaia* G magnitude at time t_n, C is a constant term, and A and φ are the amplitude and phase of the sine wave, respectively.

The former classification did not automatically exclude those variables for which ν_1 is not statistically significant. Hence, for this sample the classification may be partly based on detected variability that has no astrophysical origin. For this reason we imposed a first threshold on the false alarm probability (FAP; Baluev 2008) of ν_1, which we limit to be no greater than 0.01.

Examination of the time series revealed that a stricter FAP threshold is required for some cases. The histogram of the first frequency ν_1 for our sample of stars is shown in Fig. 1 in dark blue. This histogram shows that, although the quality of the photometric data reduction is steadily and significantly improving with every data release, the photometric data are not yet completely free of instrumental artefacts. We see high peaks around harmonics of 4 d^{-1}, which is the spin frequency of the spacecraft (cf. Gaia Collaboration 2016). The strong wings around these peaks suggest that sources in a fairly broad frequency range are affected. For these stars, the Fourier analysis therefore extracted the signature of an instrumental variation rather than an astrophysical variation. Holl et al. (2023) and Distefano et al. (2023) also observed instrumental periodic variations in the photometric data of *Gaia* DR3, be it while focusing on a different frequency range ($\nu < 0.5\,\mathrm{d}^{-1}$) from that relevant for this article. Although these authors were not able to clean the affected time series from instrumental variations, they were able to efficiently filter out the impacted sources. Their filtering method proved not as efficient for our sources, casting doubt on whether the instrumental frequencies observed at very low frequencies are of the same origin as those we observe at high frequencies. There are multiple possible reasons for this; in addition to genuine instrumental variations, some of the peaks observed in Fig. 1 might be caused by frequency aliasing of very low frequencies into high frequencies. For the final release (*Gaia* DR5), we expect the instrumental variations to be mostly calibrated out.

To mitigate these variations for the benefit of the current paper, we experimented with many different observables to filter out the affected sources. The only effective one proved to be a stricter FAP threshold, which we limit to be no greater than 10^{-3} for sources with $\nu_1 \in [4, 25]\,\mathrm{d}^{-1}$. This strongly reduces the wings of the high peaks seen in Fig. 1. It does not completely eliminate the peaks themselves, and so we also removed all sources with a frequency ν_1 near 4, 8, 12, 16, 20, and 24 d^{-1} using a proximity threshold of 0.05 d^{-1}. Lastly, we also discarded those sources with $\nu_1 < 0.7\,\mathrm{d}^{-1}$ to avoid dominant long-term variability of unknown origin, because most of the dominant g modes found in *Gaia* DR3 data of the best characterised 63 bona fide *Kepler* γ Dor and SPB stars have frequencies above this value (cf. Appendix A). The histogram of ν_1 of the resulting sample of 108 663 sources is shown in light blue in Fig. 1.

Looking further at the main frequency ν_1, we find that the CU7 classifiers assign some of the stars to the β Cep, SPB, γ Dor, or δ Sct classes even if ν_1 is far from the typical frequency ranges associated with the dominant modes of such stars in this particular type of variables, even when taking into account frequency shifts due to rapid rotation. An underlying reason is that the classifiers did not assign sufficient weight to the main frequency of the variability. In a next step we therefore further filtered the main frequency ν_1 and only retained stars classified as β Cep stars with $\nu_1 \in [3, 8]\,\mathrm{d}^{-1}$ (Stankov & Handler 2005), stars classified as δ Sct stars or SX Phe stars with $\nu_1 \in [5, 25]\,\mathrm{d}^{-1}$ (Rodríguez & López-González 2000; Rodríguez et al. 2000), stars classified as γ Dor stars with $\nu_1 \in [0.7, 3.2]\,\mathrm{d}^{-1}$ (Li et al. 2020), and stars classified as SPB stars with $\nu_1 \in [0.7, 5]\,\mathrm{d}^{-1}$ (Pedersen et al. 2021), which leaves a sample of 106 207 variables.

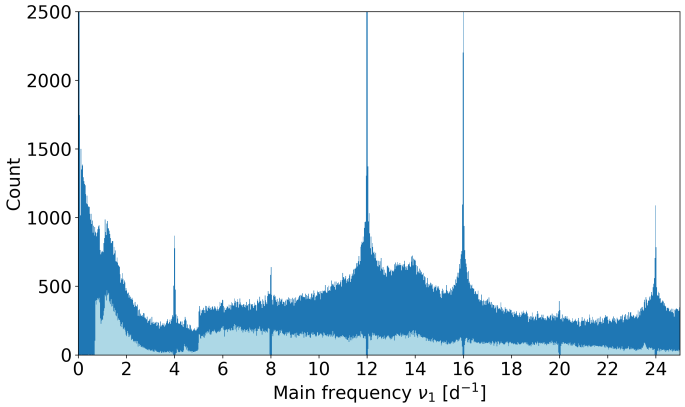


Fig. 1. A histogram of the first frequency ν_1. Dark blue: histogram of the first frequency ν_1 of the 460 519 candidate main sequence variables. The highest peaks go beyond the maximum value of the y-axis. Light blue: Same histogram for the 108 663 for which we filtered on the primary frequency ν_1 and its corresponding FAP value to avoid instrumental artefacts. Because of the 34-month time-span of the DR3 time series, the typical uncertainty on the frequency is about $10^{-3}\,\mathrm{d}^{-1}$.

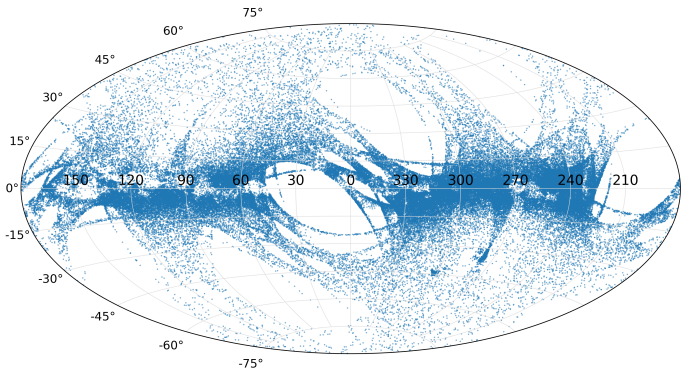


Fig. 2. Sky distribution in Galactic coordinates of the 106 207 sources in the data set resulting from various steps of filtering as described in Sect. 2.

Figure 2 shows the sky distribution of our sample in galactic coordinates, and Fig. 3 shows the projection on the XY galactocentric plane of the subset of 71 490 sources with a relative parallax uncertainty $0 < \sigma_\varpi/\varpi < 0.25$. The galactocentric coordinates $(X_{\mathrm{gal}}, Y_{\mathrm{gal}})$ were computed using the median photogeometric distances computed from *Gaia* EDR3 data by Bailer-Jones et al. (2021).

The gaps in the spatial distribution are caused by *Gaia*'s scanning law and the lower constraint on the number of time points ($N \geq 40$) for our sources.

Finally, Fig. 4 shows examples of phase diagrams of high-S/N light curves for each of the OBAF-type pulsators.

3. The IHM instability strips as observed by *Gaia*

In a global sense, pulsation theory successfully predicts the occurrence of modes in OBAF-type main sequence stars in the HR diagram (see e.g., Dupret et al. 2005; Townsend 2005;

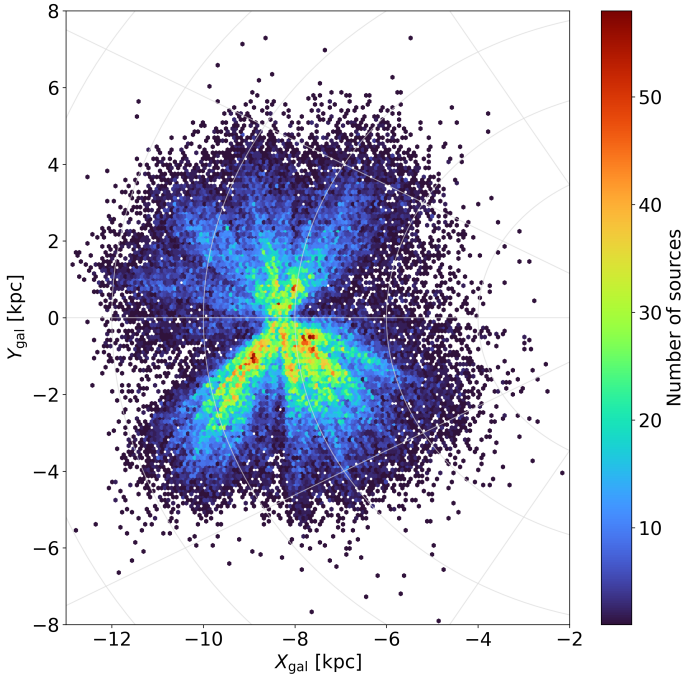


Fig. 3. Distribution of the Galactic sources of the dataset shown in Fig. 2, limited to those 71 490 stars with $0 < \sigma_\varpi/\varpi \leq 0.25$, projected on the equatorial plane of the Galactocentric reference frame.

Miglio et al. 2007; Daszyńska-Daszkiewicz et al. 2013; Xiong et al. 2016; Szewczuk & Daszyńska-Daszkiewicz 2017; Burssens et al. 2020, and references therein). However, discrepancies between mode excitation predictions and observations occur, both at the level of the observed samples as a whole and for the various detected modes in individual pulsators. As an example of the former, Murphy et al. (2019) found that the observational instability strip of about 2000 δ Sct stars detected in *Kepler* data covered a broader temperature regime than predicted by state-of-the-art pulsation theory based on time-dependent convection theory (Dupret et al. 2005). For individual hotter stars, two examples of IHM pulsators with detected modes predicted not to be excited were discussed in great detail by Daszyńska-Daszkiewicz et al. (2017) and Moravveji et al. (2015) for a β Cep and SPB star, respectively. These two B-type pulsators are representative of numerous additional cases, pointing to overly low opacities for iron peak elements used as input physics for the computation of stellar models. Moreover, even in state-of-the-art stellar models, very approximative treatments of internal rotation and core convection are used, leading to unreliable predictions about their non-radial oscillations (Aerts 2021). On the other hand, from the observational side, the empirical location of IHM stars in the HR- or Kiel diagrams is often plagued by large systematic uncertainties on the observed stellar distance, interstellar reddening, and bolometric corrections (Pedersen et al. 2020), as well as on the star's gravity, helium abundance, metallicity (z), and, to a lesser extent, effective temperature (Burssens et al. 2020; Gebruers et al. 2021).

For the present *Gaia* sample, we face the additional challenge that the classification was based on one frequency only, which makes the presence of contaminants in our sample likely. In particular, rotationally modulated stars are prevalent at spectral types A and B (e.g., Bp and Ap stars, Kurtz 2000; Briquet et al. 2007; Balona et al. 2011b; Bowman et al. 2018). Bp and Ap stars tend to be slow to moderate rotators showing surface spots, leading to variability in the same frequency domain as g-mode pulsations. On top of that, although the window function of *Gaia* time series is significantly better than those of typical ground-based surveys, the highest peak in the normalised spectral window of the *Gaia* DR3 time series can still reach 60% or more for certain regions in the sky. We cannot therefore exclude that a fraction of the low-frequency oscillators are actually δ Sct or β Cep stars for which an alias frequency was found instead of the true frequency. Likewise, high-frequency oscillators might have been classified as SPB or γ Dor star because of frequency aliasing (cf. Appendix A).

For our sample of OBAF-type IHM stars, we extract the effective temperature $T_{\rm eff}$ from the field `teff_gspphot` in the table `astrophysical_parameters_supp` in *Gaia* DR3. The luminosities were computed using the absolute G magnitude `mg_gspphot` field in the same table, and a bolometric correction BC (depending on $T_{\rm eff}$) from Pedersen et al. (2020) for stars hotter than 10 000 K and from Eker et al. (2020) for the cooler stars. In both cases, we used the metallicity-independent BC prescription, as we do not have a reliable estimate of $[M/H]$ for most of our stars. We propagated the errors on $T_{\rm eff}$ and M_G to obtain the errors on the bolometric corrections and the luminosities. The typical $T_{\rm eff}$ uncertainty of the stars in our sample as reported in table `astrophysical_parameters_supp` is about 150 K, leading to a typical uncertainty of 0.08 on $\log L$. However, as Andrae (2023) discusses in depth, the uncertainties on $T_{\rm eff}$ and M_G in the *Gaia* DR3 release are likely underestimated, in some cases by a factor of three. Given the experience of ground-based spectroscopy, we can expect a minimum uncertainty of about 400 K on $T_{\rm eff}$, especially for the hotter B-type pulsators.

As our sample includes stars from magnitudes $G = 6$ to $G = 18$, and the uncertainty on the `gspphot` stellar parameters is often too large to make them useful for placement in the HR diagram, we limit ourselves to the nearby IHM pulsators with a relative *Gaia* DR3 parallax uncertainty $0 < \sigma_\varpi/\varpi < 0.03$. Figure 5 shows a HR diagram with the nearby *Gaia* sources classified as γ Dor or SPB as described in Sect. 2. In the same figure, the SPB-star instability strip from Burssens et al. (2020) is plotted ($\ell \in \{0, 1, 2\}$, $n \in \{-50, \ldots, -1\}$, $Z = 0.02$) along with the γ Dor instability strip ($\ell = 1$, $Z = 0.02$) from Dupret et al. (2005) for a value of the mixing length, $\alpha_{\rm MLT} = 2$.

The highest concentration of g-mode pulsators is, as expected, inside the γ Dor instability strip. The slight offset towards lower luminosities is easily explained as due to systematic uncertainties in the reddening or bolometric correction BC. The low-frequency variables blueward of the γ Dor instability strip fall inside or above the δ Sct instability strip (cf. Fig. 6). Aside from the possibility that they might be hot γ Dor stars (Li et al. 2020) or γ Dor stars with an uncertain location in the HR diagram, they could also represent hybrid p- and g-mode γ Dor/δ Sct pulsators (Grigahcène et al. 2010; Bowman et al. 2016), aliased δ Sct stars, Bp/Ap stars (Balona et al. 2019), fast-rotating SPB stars (Townsend 2005; Szewczuk & Daszyńska-Daszkiewicz 2017), or rotationally modulated g-mode pulsators following the recent pulsation excitation theory for fast rotating early-type stars (Ouazzani et al. 2020; Lee & Saio 2020; Lee 2021). This latter theory predicts g-mode pulsators to occur in rapid rotators between the SPB and γ Dor instability strips, that is, at effective temperatures representative of spectral types A0–A3. This concerns fast rotating spotted stars with gravito-inertial envelope modes coupled to inertial core modes as observed in *Kepler* observations (Saio et al. 2018).

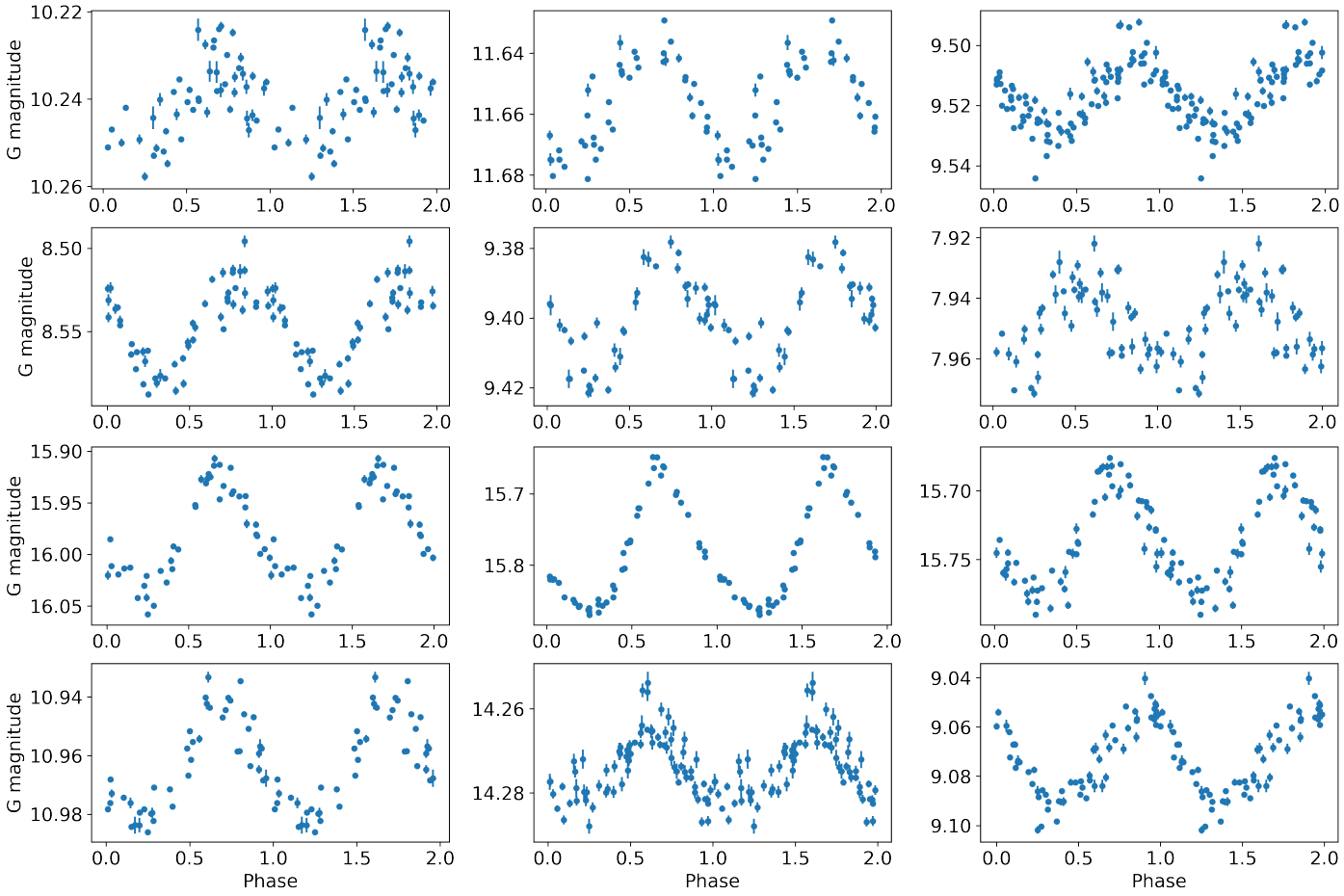


Fig. 4. Example phase diagrams of sources classified as main sequence OBAF-type pulsators, folded with the primary frequency ν_1 found in *Gaia* G-band photometry. *From top to bottom* the rows show three examples of stars classified as respectively β Cep, SPB, δ Sct, and γ Dor variables.

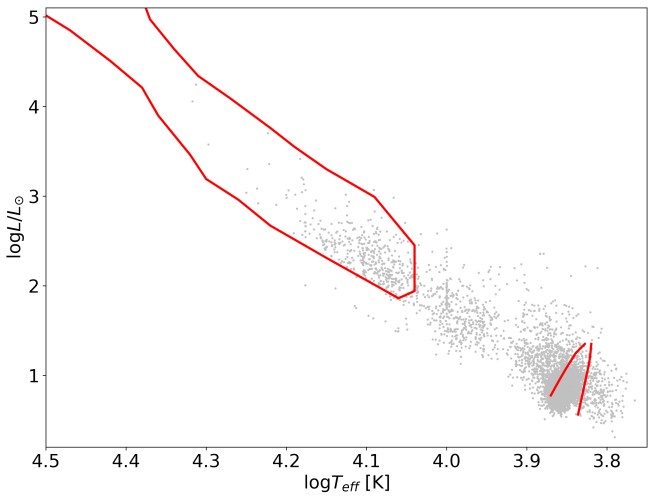


Fig. 5. HR diagram of 10 402 nearby g-mode pulsators classified as SPB or γ Dor star with a relative parallax uncertainty of better than 3%. The red line is the SPB instability strip from Burssens et al. (2020, at hot temperatures) and the γ Dor instability strip from Dupret et al. (2005, at low temperatures), both for solar metallicity.

Occurrences of rapidly rotating g-mode pulsators between the SPB and δ Sct instability strips are well established from modern space photometry. Indeed, after initial discoveries from CoRoT data of SPB stars (Degroote et al. 2009, 2011), numerous detections were achieved from ground-based cluster studies as well (Saesen et al. 2010, 2013; Mowlavi et al. 2013, 2016; Moździerski et al. 2014, 2019; Saio et al. 2017). These detections are interpreted as fast-rotating SPB stars from instability computations based on the so-called traditional approximation of rotation applied to g modes (Salmon et al. 2014), following the interpretation by Aerts & Kolenberg (2005) based on spectroscopic time-series data. Many fast-rotating SPB and Be pulsators were also found near the red edge or below the SPB instability strip from *Kepler* and TESS data (Balona et al. 2011a; Pedersen et al. 2019; Burssens et al. 2020; Sharma et al. 2022). Our *Gaia* results in Fig. 5 reveal plenty of g-mode pulsators between the SPB and δ Sct instability strips. Within this group of g-mode pulsators, we observe an under-density between the hot A stars and the blue edge of the δ Sct instability strip. At this point, we cannot exclude that this is an artefact rather than having an astrophysical origin.

The distribution of stars within the SPB instability strip in Fig. 5 is concentrated in or near the cooler bottom half, in close agreement with mode density excitation predictions (cf. Fig. 1 in Pápics et al. 2017). These g-mode pulsators are in the same position as those observed in high-cadence space photometry of slow- and fast-rotating B and Be stars (Neiner et al. 2009, 2012; Huat et al. 2009; Diago et al. 2009; Baade et al. 2016, 2018a,b; White et al. 2017; Pedersen et al. 2019, 2021; Burssens et al. 2020; Szewczuk et al. 2021; Sharma et al. 2022). It is noteworthy that the *Gaia* CU7 classification scheme also has a class of γ Cas

variables representing classical Be stars (Rivinius et al. 2013). It has long since been known from line-profile variability that many Be stars are rapidly rotating non-radial p- and/or g-mode pulsators (Rivinius et al. 2003). High-cadence space photometry indeed reveals most of the γ Cas variables to have non-radial pulsations aside from rotational modulation (Balona et al. 2011a; Balona 2016), including the prototype γ Cas itself (Labadie-Bartz et al. 2021; Smith & Henry 2021). We did not include the γ Cas variables in our study, because this class definition within CU7 does not rely on them being non-radial pulsators. We therefore anticipate that many more rapidly rotating non-radial B-type pulsators occur in *Gaia* DR3, but were assigned to the γ Cas class.

In Fig. 6 we show the HR diagram dedicated to the stars that were classified as either β Cep or δ Sct stars. As before, we imposed a relative parallax of better than 3% for the δ Sct stars. For the β Cep stars, which are much more rare, we relaxed this constraint to $0 < \sigma_\varpi/\varpi < 0.2$. The vast majority of δ Sct stars are well concentrated in the expected instability strip of p modes, demonstrating both the good performance of the variability classifier as well as the precision of the astrophysical parameter determination by the CU8 processing pipeline, at least for the nearby stars. Higher up the main sequence, the sample of nearby very luminous β Cep stars is small. Most of them have an observed location in the HR diagram outside the expected instability strip, which is difficult to explain in terms of metallicity. The most likely explanation is a systematic bias in the astrophysical parameters of hot stars as derived from *Gaia* DR3 `gspphot` data. Indeed, the observed shifts to cooler temperatures can easily occur due to poorly estimated reddening. However, the effects of fast rotation may also play a role, as it is not or only incompletely treated in published instability strips for p modes, while its impact on the properties of the modes is large (Daszyńska-Daszkiewicz et al. 2002). Many fast rotators with p modes have indeed been found in high-cadence space photometry of early-type B and Be stars (Balona et al. 2011a; Burssens et al. 2020; Balona & Ozuyar 2020).

The classifier also picked up a sample of stars with high frequencies ν_1 right below the SPB instability strip, with $T_{\rm eff}$ around 10 000 K or slightly cooler. These variables are in line with CoRoT and TESS discoveries of what appears to be p-mode pulsators in that position of the HR diagram (Degroote et al. 2009; Balona & Ozuyar 2020). The variability of such pulsators is not yet well understood. We note that the frequencies of gravito-inertial modes in moderate to fast rotators can easily get shifted into the regime of p modes (e.g., Aerts & Kolenberg 2005; Salmon et al. 2014). Such frequency shifts may be particularly large for g modes with $|m| > 1$, which complicates the classification of the variability based on the frequencies from photometry alone. This is illustrated nicely by the two cases of the slowly rotating variable star Maia (Struve 1955) and the magnetic moderately rotating SPB pulsator HD 43317 (Pápics et al. 2012). While Maia was originally classified as a pulsator by Struve (1955) and even led Struve to introduce a seemingly new class of pulsators (the so-called Maia variables), White et al. (2017) showed it to be a rotationally modulated star rather than a pulsator. On the other hand, the high-frequency mode of HD 43317 at 4.3 d^{-1} was originally misinterpreted as a p mode, while it is a rotationally shifted quadrupole g mode (Buysschaert et al. 2018). These two examples reveal that misclassifications of B-type variables based on photometric data alone are easily made and that correct interpretation of the frequencies of such stars in the regime of a few to several d^{-1} is only possible from adding independent data – such as high-precision spectroscopy – to photometric light curves. Given the recent *Kepler*-guided understanding of fast rotating BAF-type pulsators with mode frequencies between pure g and pure p modes, such variables were not yet included as a separate variability class in the CU7 classifiers. Therefore, their strongly shifted non-radial mode frequencies due to fast rotation in the inertial frame of the observer may imply that these variables get spuriously classified as p-mode pulsators below the SPB instability strip in Fig. 6.

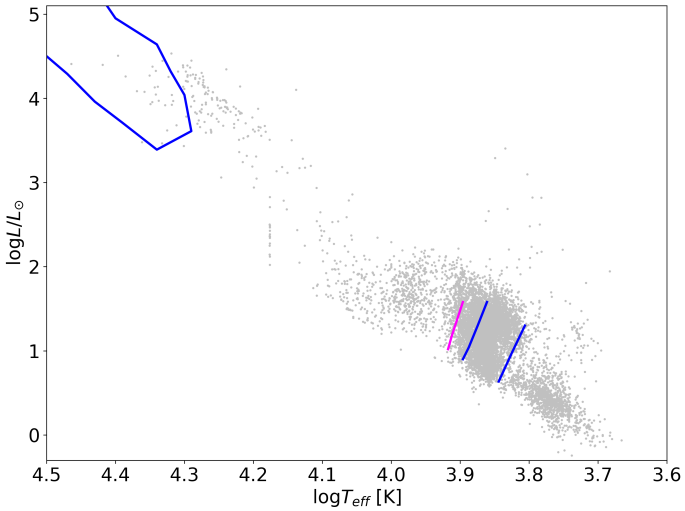


Fig. 6. HR diagram of 13 974 nearby p-mode pulsators classified as β Cep or δ Sct stars. For the β Cep stars, we imposed $0 < \sigma_\varpi/\varpi < 0.2$, while we demanded $0 < \sigma_\varpi/\varpi < 0.03$ for the δ Sct stars. The blue line at hot temperatures is the β Cep star instability strip from Burssens et al. (2020) for spherical degree $\ell \in \{0, 1, 2\}$ and radial order $n \in \{0, \ldots, 6\}$. The blue lines represent the blue and red edge of the δ Sct instability strip for $n = 1$ modes, and the fuchsia line the blue edge for $n = 4$ modes. All instability strips are for solar metallicity.

An even larger overdensity of high-frequency variables also pops up at cooler temperatures well below the δ Sct instability strip. A closer look at this part of the HR diagram is shown in Fig. 7. This concerns mainly stars with dominant frequency below 7 d^{-1}, obeying a period–luminosity relation (albeit a noisy one) as can be seen from the colour gradient in the figure. We postulate that this may be a cooler-temperature, lower mass relation analogous to the period–luminosity (PL) relations found for rapidly rotating B-type pulsators with g modes occurring below the SPB instability strip. Such PL relations were initially deduced by Saio et al. (2017) based on the B-type cluster pulsators found by Mowlavi et al. (2013, 2016). Sharma et al. (2022) found similar PL relations from TESS photometry of rapidly rotating g-mode pulsators occurring between the SPB and δ Sct strips (cf. Fig. 5). Sharma et al. (2022) interpreted these PL relations in terms of dipole ($l = |m| = 1$) and quadrupole ($l = |m| = 2$) g modes. It may well be that the PL relation revealed in Fig. 7 can be explained similarly, that is, as the result of a mixture of dipole or quadrupole gravito-inertial, Rossby, or Yanai modes in very fast rotators of spectral type F, as such types of modes have been detected in *Kepler* photometry of cool γ Dor stars (Van Reeth et al. 2016, 2018; Saio et al. 2018).

4. Comparison with the literature

Starting from our 106 K sample described in Sect. 2, we removed the distinct population of stars far beyond the red edge of the δ Sct instability strip (cf. Fig 7 for a nearby subsample of them), as we cannot rule out the possibility that these are

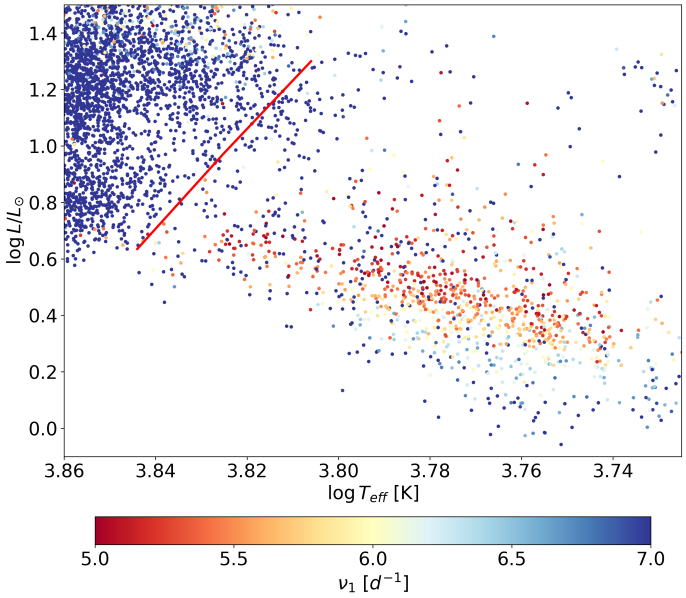


Fig. 7. Zoom into the overdensity below the δ Sct instability strip at lower effective temperatures in the HR diagram shown in Fig. 6. The red line is the red edge of the δ Sct instability strip for $n = 1$ modes.

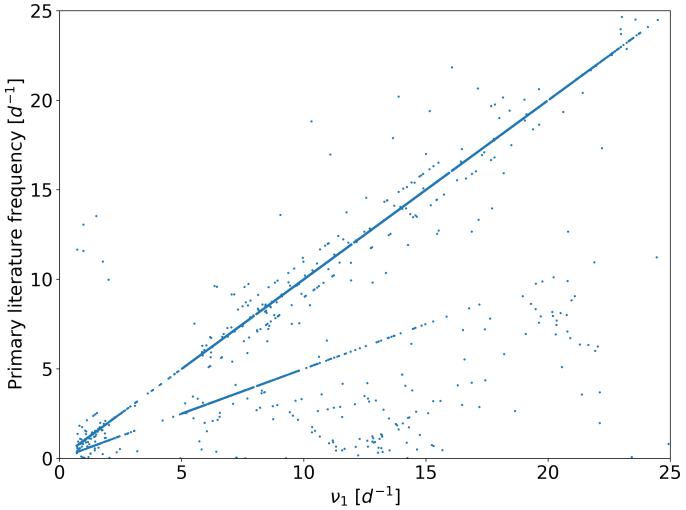


Fig. 8. Comparison with the main frequency ν_1 found with the CU7 pipeline using *Gaia* DR3 data and the main frequency f_1 reported in the literature.

misclassifications at this point. This leaves us with a sample of 88 872 sources, which in the remainder of this section we refer to as the 88 K sample.

We compare our sample of 88 K candidate IHM main sequence oscillators with two different compilations from literature catalogues. The first compilation consists of 2121 δ Sct stars and 603 γ Dor stars in the *Kepler* field as identified by Bowman et al. (2016), Murphy et al. (2019) and Van Reeth et al. (2015), Li et al. (2020), respectively. This sample has the advantage that the classification was carried out manually based on dense *Kepler* time series, and is therefore very reliable. The drawback is that the sample covers only the fairly small magnitude range observed by *Kepler* and is very localised in the sky. This sample therefore does not cover the large magnitude range of our *Gaia* DR3 sample, nor does it cover all the window functions caused by the sky-coordinate-dependent *Gaia* sampling.

Focusing first on the δ Sct stars, we find that 746 of them (35%) are identified as an OBAF-type pulsator by the CU7 classifiers. The majority were therefore either not found to be variable in the time domain or ended up as another type of variable. This illustrates the challenges that come with identifying these small-amplitude multi-periodic variables with the fairly small number of *Gaia* measurements. Of these 746 pulsators, 73 (10%) have a FAP of smaller than our threshold of 10^{-3} (cf. Sect. 2). Our measures to mitigate the presence of instrumental effects have a significant impact on the selection of bona fide pulsators as well. The vast majority (82%) of the δ Sct stars that did pass the FAP criterion were correctly identified as δ Sct stars by the CU7 classifiers.

The results for the γ Dor stars are similar. We find that 233 of them (39%) passed the CU7 classifier as an OBAF-type pulsator, and 26 of these stars have a FAP value smaller than our threshold of 10^{-2} for g-mode pulsators. For most of these stars, their small amplitudes (often below 5 mmag, cf. Appendix A) make the peaks in the Fourier spectrum barely statistically significant and distinguishable from peaks purely caused by noise fluctuations.

The second literature compilation with which we compare our sample is that of Gavras et al. (2023), who compiled a large database of variable stars using existing catalogues published in the literature (before the *Gaia* DR3 release), including those of Stankov & Handler (2005), Pigulski & Pojmański (2009), Palaversa et al. (2013), Drake et al. (2017), and Chen et al. (2020) among others. The compilation ensured an all-sky coverage and a large range of G magnitude (and thus S/N levels). It consists of catalogues compiled using a manual variability classification, as well as catalogues based on a probabilistic machine learning approach. We refer to Gavras et al. (2023) for more details. Although these latter authors adopted a stringent classification score threshold, we should expect a small fraction of these literature classifications to be inaccurate.

For 12 042 stars in our sample, the cross-match catalogue of Gavras et al. (2023) includes a primary frequency found in the literature. The comparison of these literature frequencies with the ones derived by CU7 using *Gaia* DR3 photometric time series in the G passband is shown in Fig. 8. Overall there is an excellent match between the *Gaia* DR3 and the literature frequencies. A small sample of sources forms a parallel line above and below the main diagonal. These are sources for which ground-based observations found a one-day alias of the true frequency, while the oscillation frequency found by *Gaia* is not affected by Earth's day–night rhythm. For a smaller sample, the main frequency derived from *Gaia* DR3 data is twice the frequency found in the literature. We find that most of them are stars catalogued as a binary star in the literature, but erroneously classified as a g-mode pulsator by the CU7 classifiers.

The literature cross-match compilation of Gavras et al. (2023) contains 108 β Cep stars, 98 SPB stars, 421 γ Dor stars, and 14350 δ Sct stars (+SX Phe) for which the corresponding source in *Gaia* DR3 has at least 40 data points, and which could therefore in principle have been retained after the data selection criteria explained in Sect. 2. Of these stars, 41 β Cep stars (38%), 49 SPB stars (50%), 69 γ Dor stars (16%), and 9780 δ Sct + SX Phe star (68%) also appear in our *Gaia* DR3 sample of 88 K variables. Of this subselection the CU7 classification pipeline obtained the same classification as the literature for 41 β Cep stars (100%), 42 SPB stars (86%), 64 γ Dor stars (93%), and 9765 δ Sct stars (99.8%). The miss rate (i.e. the false negative

rate FN/(FN + TP)) is therefore fairly good for δ Sct stars (32%) but high (≥57%) for the other OBAF-type pulsators. This is not surprising, given that the stars in our 88 K sample have a median number of time points equal to 56. Nevertheless, the OBAF-type pulsators of the literature that do end up in our 88 K sample are mostly correctly classified. We remind the reader that the CU7 classification pipeline used XGBoost and Random Forest classifiers to classify 12 million variable stars into 25 variability classes. More details can be found in Rimoldini et al. (2023).

Starting from our 88 K sample of *Gaia* DR3 OBAF-type pulsators, it turns out that 66 β Cep stars, 119 SPB stars, 793 γ Dor stars, and 11064 δ Sct (+SX Phe) stars also appear in the literature compilation of Gavras et al. (2023), although not necessarily classified as the same type. For the β Cep stars, the main contaminants are the γ Cas variables (20%) and the δ Sct variables (6%). For SPB stars, the main contaminants are α^2 Canum Venaticorum (ACV) variables (24%), rotationally modulated stars (21%), and γ Cas variables (9%). The γ Dor stars are confused most often with RS Canum Venaticorum variables (33%), rotationally modulated stars (23%) and, as expected, with binary stars (12%). Finally, the δ Sct (+SX Phe) stars are sometimes confused with binaries (6%), RR Lyr stars (2%), or RS Canum Venaticorum variables. Assuming again that the literature class label is always reliable, we can conclude that the false discovery rate (i.e. FP/(FP+TP)) is fairly good to excellent for the high-frequency variables, as low as 12% for the δ Sct stars, but is high for the low-frequency variables (≥65%). However, we note that we used our entire 88 K sample for this assessment, including the faint stars. As can be seen from the previous section, the comparison gives much better results for the nearby and brighter stars.

To investigate why the classification of g-mode pulsators is so difficult with *Gaia* DR3 data in more detail, we analyse in Appendix B the *Gaia* DR3 time series in the *Gaia* G-band for 63 well-known bona fide g-mode pulsators listed in Aerts et al. (2021). For these stars, we know the true oscillation frequency from densely sampled *Kepler* photometric time series. Our analysis confirms the comparison with the literature above. For about 15% of these stars, the main frequency identified from *Gaia* photometry coincides with the main frequency found from *Kepler* photometry. For two of these stars, the second frequency also coincides. The main culprit for mismatches is either an aliased frequency making the g-mode pulsator look like a δ Sct star, or an instrumental frequency as described in Sect. 2.

5. The period–luminosity relation of δ Sct stars

δ Sct stars pulsating in the radial fundamental (F) and/or in the first overtone (1O) mode show a period–luminosity relation, albeit with a larger scatter than for Cepheids (see e.g., McNamara et al. 2007; McNamara 2011; Ziaali et al. 2019; Jayasinghe et al. 2020; Poro et al. 2021). For these modes, the pulsation constant $Q \equiv P\sqrt{\bar{\varrho}/\bar{\varrho}_\odot}$ is more or less constant over the instability strip, and the dominant stellar property that correlates with the stellar mean density is the luminosity L, hence the PL relation (Breger 2000).

To establish the relation as seen using the *Gaia* DR3 dataset, we first computed the reddening-insensitive period–Wesenheit (PW) relation. The absolute Wesenheit index W was computed using

$$W = M_G - 1.9\,(G_{\rm BP} - G_{\rm RP}), \tag{2}$$

where M_G is the absolute magnitude in the G-band taken from the *Gaia* DR3 `astrophysical_parameters` table (`gspphot`).

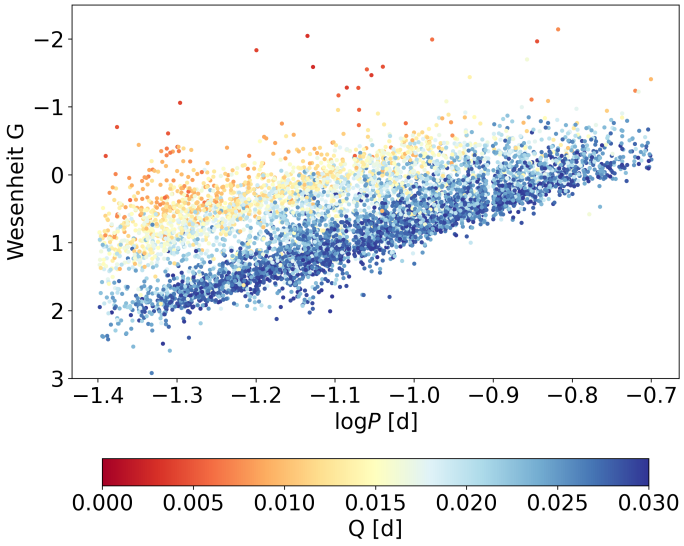


Fig. 9. Period–Wesenheit relation for 6511 δ Sct stars with $\sigma_\varpi/\varpi < 0.05$, $T_{\rm eff} \in [6400, 8700]$ K, and $Q < 0.03$. The uncertainty on $\log P$ is smaller than the symbol size. The typical uncertainty of the Wesenheit G index is between 2 and 4 mmag.

Inspection of the PW relation obtained with this sample revealed some contamination from the well-defined group of low-luminosity stars with a frequency $f < 6.6\,{\rm d}^{-1}$ ($P > 0.15$ days) described in the last paragraph of Sect. 3. Because of their compactness, it proved easy to select and remove them with the criteria $f < 6.6\,{\rm d}^{-1}$ and $W < 1.0$ mag. In this way, we discarded 233 objects. Figure 9 shows the PW relation for nearby δ Sct stars with $\sigma_\varpi/\varpi < 0.05$ and $T_{\rm eff} \in [6400, 8700]$ K colour coded with the empirical Q value (in days). The latter was computed using the relation derived by Breger (1990):

$$\log_{10}\left(\frac{Q}{P}\right) = -0.25\log_{10}\left(\frac{L}{L_\odot}\right) + 0.5\log_{10}\left(\frac{g}{g_\odot}\right) + \log_{10}\left(\frac{T_{\rm eff}}{T_{\rm eff,\odot}}\right). \tag{3}$$

As before, the quantities $L/L_\odot$, g and $T_{\rm eff}$ were taken from the *Gaia* DR3 `astrophysical_parameters` table (`gspphot`). Comparing the empirical pulsation constant Q with the typical values given by Breger (1979), we see that the *Gaia* DR3 data not only show the ridge of the fundamental mode (dark blue), but also the ridges of the first and the second overtone.

In the remainder of this section, we focus on the most populous ridge in Fig. 9 which is that of the fundamental mode pulsators, for which we follow a more precise procedure. The high-amplitude δ Sct (HADS) variables are known to pulsate in the F mode, the 1O mode, or both (McNamara et al. 2007). Figure 10 shows a histogram of the amplitude $A_{G,1}$ of the main frequency ν_1 for our sample of δ Sct stars, in which the HADS population is clearly visible. To avoid too much contamination of the non-radially pulsating lower amplitude population, we only retained δ Sct stars with $A_{G,1} \geq 50$ mmag. As before, we constrained the effective temperature of our sample stars to the range of the δ Sct instability strip, i.e. $6400\,{\rm K} \leq T_{\rm eff} \leq 8700$ K. This left us with 8894 stars. In addition we also filtered on the quality of the astrometric parallax as this is a key ingredient in the derivation of the PW relation. To do so, we followed the approach of Rybizki et al. (2022), who used a neural network based on 17 proper *Gaia* catalogue entries to discriminate objects with poor astrometry by means of a single parameter which they

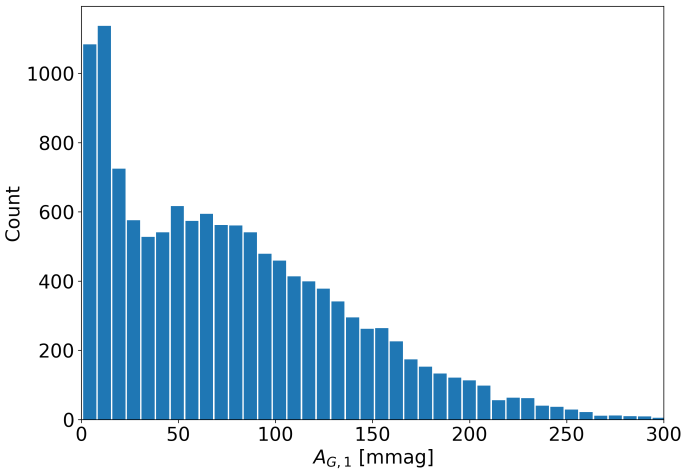


Fig. 10. Histogram of the amplitude $A_{G,1}$ of the main frequency ν_1 of our sample of δ Sct stars.

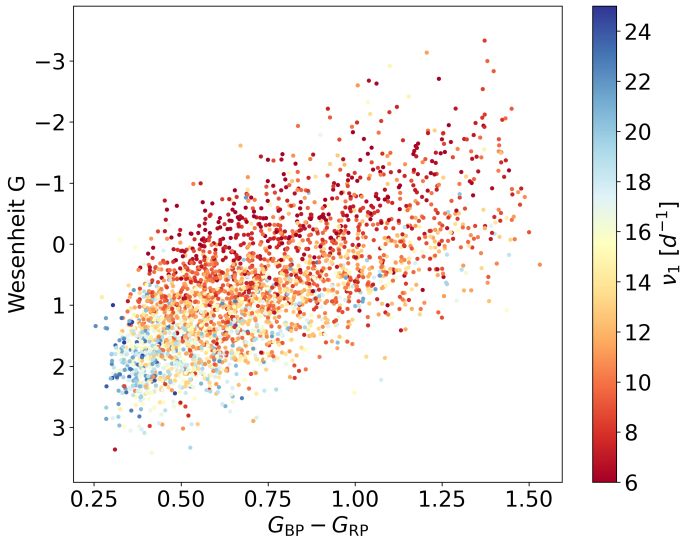


Fig. 11. Location of 3122 high-amplitude δ Sct stars with $0 < \sigma_\varpi/\varpi < 0.2$ in a colour–Wesenheit G diagram. The points are colour coded according to frequency ν_1. Typical uncertainties of the mean $G_{BP} - G_{RP}$ are between 1 and 2 mmag and between 2 and 4 mmag for the Wesenheit G index.

called 'astrometric fidelity'. We retained only objects with their `fidelity_v2` > 0.5. This last selection defined our final sample of 8760 δ Sct stars useful for the PW relation determination. We plotted the δ Sct stars in this sample with a relative parallax uncertainty of better than 20% in Fig. 11. The points are colour coded with the frequency ν_1 so that the frequency gradient due to the period–luminosity relation is clearly visible.

To calculate the PW relation, we adopted the so-called photometric parallax (see Riess et al. 2021, and references therein), which was recently used to derive the period–Wesenheit–metallicity relation for the classical Cepheids in the *Gaia* bands by Ripepi et al. (2022). This approach allows us to use the parallax linearly, retaining the Gaussian property of its uncertainty. Moreover, as we do not make any selection in parallax (even negative parallaxes can be used) we are not introducing biases in the PW relation. The photometric parallax (in mas) is defined as follows:

$$\varpi_{\rm phot} = 10^{-0.2\ (w-W-10)}, \tag{4}$$

where W is the absolute Wesenheit magnitude in the G passband, and w is the corresponding apparent Wesenheit magnitude:

$$w = G - 1.9\,(G_{\rm BP} - G_{\rm RP}). \tag{5}$$

The absolute Wesenheit index W can be written as

$$W = \alpha + \beta\,(\log_{10} P - \log_{10} P_0), \tag{6}$$

where P is the period and P_0 a 'pivoting' period (in days) chosen approximately as the mean of the period distribution (i.e. $\log_{10} P_0 = -1.1$). This serves to reduce the correlation between the zero point α and the slope β of the PW relation.

Denoting with $\varpi_{\rm EDR3}$ the parallaxes of the pulsators corrected for the zero-point offset (ZPO) (see Lindegren et al. 2021), we seek to minimise the following quantity:

$$\chi^2 = \sum \frac{(\varpi_{\rm EDR3} - \varpi_{\rm phot})^2}{\sigma^2}, \tag{7}$$

where $\sigma^2 = \sigma^2_{\varpi_{\rm EDR3}} + \sigma^2_{\varpi_{\rm phot}}$. In our case, $\sigma_{\varpi_{\rm EDR3}}$ is composed of the standard error of the parallax as reported in the *Gaia* EDR3 catalogue, here conservatively increased by 10%, and the uncertainty on the individual ZPO corrections, that is 13 µas (Lindegren et al. 2021). To calculate the uncertainty on the photometric parallax we followed the procedure detailed by Ripepi et al. (2022): $\sigma_{\varpi_{\rm phot}} = 0.46 \cdot \sigma_\mu \cdot \varpi_{\rm phot}$, where $\mu = w - W$ is the distance modulus and $\sigma^2_\mu = \sigma^2_w + \sigma^2_W$ its variance. We calculated σ_w from error propagation assuming a constant error of 0.01 mag in each of the three *Gaia* bands (G, $G_{\rm BP}$, $G_{\rm RP}$), where σ_W is the intrinsic dispersion of the PW relation. Similarly to the case of classical Cepheids, we assumed a value of 0.1 mag for this quantity.

We minimised Eq. (7) using the `Python` minimisation routine `optimize.minimize` (included in the `Scipy` package Virtanen et al. 2020). To provide robust uncertainties on the coefficients α and β of the PW relation, we used a bootstrap procedure in which we repeated the fit to the data of Eq. (7) 1000 times, each time with a randomised bootstrap sample, and obtained a different α and β value for each repetition. Our best estimate for these two parameters is then the median of the resulting distributions, while for the uncertainty we used 1.4826 · MAD (median absolute dispersion).

In a first attempt, we fitted the PW relation over the whole period range of 0.04–0.20 days, but it became clear that a single linear fit is not able to represent the empirical PW relation as the data show a break or a non-linearity (see Fig. 12). We therefore applied two approaches, first fitting the PW with a piecewise linear function, and then with a quadratic PW relation of the form

$$W = \alpha + \beta\,(\log P - \log_{10} P_0) + \gamma\,(\log P - \log_{10} P_0)^2. \tag{8}$$

For the piecewise linear model, we find that the breaking point occurs approximately at $\log P = -1.05 \pm 0.05$. The best piecewise linear fit to the data is shown in the top panel of Fig. 12 and the corresponding fitted parameter values are listed in the first two rows of Table 1. The quadratic PW relation fit to the data is shown in the bottom panel of Fig. 12, while the corresponding fit parameters are listed in the bottom row of Table 1.

As for the piecewise linear fit, the slopes obtained for the two intervals of the dominant pulsation period are different with a significance of about 10σ, indicating that the PW relation of the δ Sct stars with a pulsation period P shorter than ~0.09 days has a much steeper slope than the one valid for the longer-period

pulsators. Also, the quadratic term has a high significance, indicating that the non-linearity or the two-regime nature of the δ Sct PW relation is a genuine physical feature.

It is instructive to compare the δ Sct PW relation with that of classical Cepheids as both classes of pulsators pulsate due to the well-known κ mechanism. Therefore, the instability strip of the δ Sct stars can be considered the low-luminosity extension of the classical Cepheid instability strip. To make the comparison, we considered the classical Cepheids' PW relations obtained in the *Gaia* bands by Poggio et al. (2021), which were derived in the same way as for the δ Sct stars in this paper. Figure 13 shows the same δ Sct stars and PW relations as in the top panel of Fig. 12 with, in addition, the location of the *F*- and 1O-mode classical Cepheids and the relative PW relations from Poggio et al. (2021). For clarity, we only show objects with relative errors on the *Gaia* EDR3 parallax of better than 20%. The distribution of the classical Cepheids pulsating in the first overtone extends up to that of the δ Sct *F*-mode pulsators[1]. It is clear that the PWs of both variability classes predict similar luminosities for modes in the period range ~0.20–0.25 days, where the δ Sct and classical Cepheid period distributions overlap. The slopes of the *F*- and 1O-mode classical Cepheids PW relations as calculated by Poggio et al. (2021) are -3.317 ± 0.028 and 3.624 ± 0.017, respectively. Comparing these values with those listed in the first two rows of Table 1, we find that the slopes for the relations found for the classical Cepheids are intermediate between those calculated for the low- and high-period δ Sct samples. If we were to ignore the observed curvature in the δ Sct PW data and fit a single straight line, this would produce an intermediate slope similar to that of the classical Cepheids.

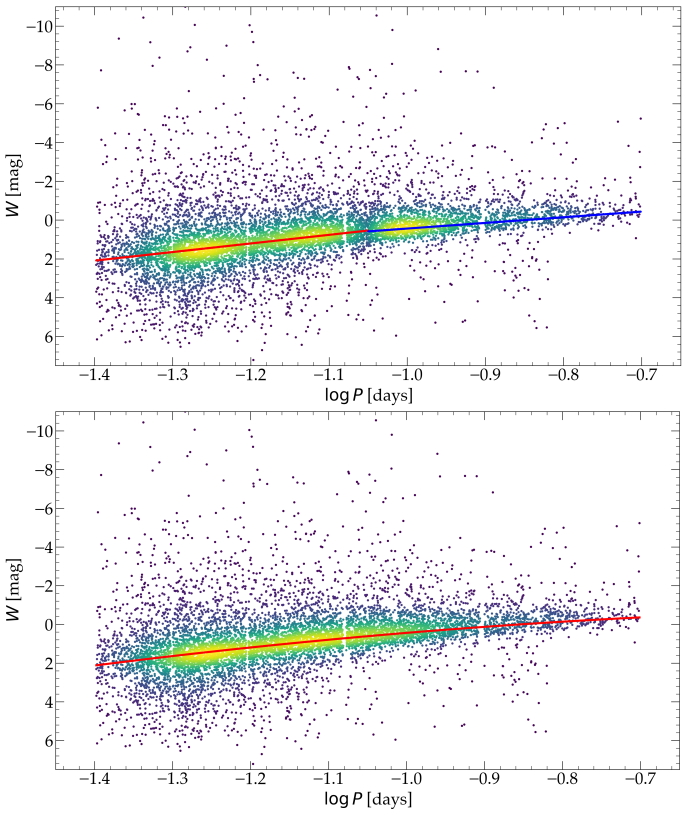


Fig. 12. PW fit to the data. The *top panel* shows the two-line fit (see first two lines of Table 1) and the *bottom panel* shows the quadratic fit to the data (see first two lines of Table 1).

6. Pulsation amplitude attenuation due to rotation

There are at least two ways in which stellar rotation can affect the observed photometric oscillation amplitudes[2]. The first is through a change in the photometric visibility, that is, how the pulsation manifests itself on the stellar surface, and the second is through a change in the intrinsic oscillation amplitude. Theoretical predictions of photometric visibilities for modes in rotating stars have been analysed in depth in the literature (see e.g., Daszyńska-Daszkiewicz et al. 2007 and Reese et al. 2013, 2021 for p modes and Henneco et al. 2021; Dhouib et al. 2021a,b for g modes). For non-radial oscillations in fast rotators, the surface pattern of the modes can no longer be described by a single spherical harmonic Y_ℓ^m. Depending on the type of mode, its frequency, and the angular rotation speed, the pulsation patterns can have a complex structure making them appreciable only at certain latitudes, which affects the geometrical disc-integration factor.

The effect of rotation on the intrinsic amplitude of κ-driven pulsators is poorly understood. The vast majority of available pulsation codes rely on linear pulsation theory, which does not allow the mode amplitudes to be derived. Analysing the effect of rotation on the pulsation amplitudes in rapidly rotating IHM pulsators requires non-linear pulsation theory, which takes into account the effects of mode coupling in the presence of the Coriolis and centrifugal forces. While nonlinear mode coupling is detected in many IHM pulsators (Bowman et al. 2016; Van Beeck et al. 2021), modelling of their observed mode amplitudes has not yet been achieved.

Observations suggest that there is a link between the rotation of a star and its photometric pulsation amplitudes, but the relationship between the two is not well understood (e.g., Aerts et al. 2014, in the case of B-type pulsators). This is partly due to the limited sample sizes of IHM pulsators with the appropriate information. Given the sample sizes of new IHM pulsators presented here, and the precision of $v \sin i$ delivered by *Gaia* for these stars, we focus here on the observed relationship between rotation and amplitude of the dominant pulsation mode for the δ Sct stars. The extreme case of the δ Sct star Altair rotating at an equatorial speed of $\sim 310\,\mathrm{km\,s^{-1}}$ (Bouchaud et al. 2020) reveals a high level of complexity in its pulsations (Le Dizès et al. 2021) and makes a study of the relationship between mode amplitudes and rotation for an entire sample worthwhile.

The high-amplitude δ Sct stars tend to rotate slower (typically $v \sin i \leq 30\,\mathrm{km\,s^{-1}}$) than normal δ Sct stars, which tend to have $v \sin i \geq 150\,\mathrm{km\,s^{-1}}$ (see e.g., Breger 2000; Antoci et al. 2019). This suggests that different angular momentum transport mechanisms are at work in these two groups of δ Sct stars, or different efficiencies of the same mechanism. The origin of this transport is poorly understood (Aerts et al. 2019). To investigate the relation between the oscillation amplitude and the stellar rotation, we cross-matched the stars classified as δ Sct stars in our sample described in Sect. 2 with those in the *Gaia*-DR3 archive for which a $v \sin i$ value is available from *Gaia* spectroscopy (`vsini_esphs`) with a formal precision better than 50%. This returned 3515 sources, which we partitioned into ten bins in $v \sin i$, each with a width of $15\,\mathrm{km\,s^{-1}}$. For each bin, we computed the median value of the photometric amplitude $A_{G,1}$.

[1] The instability strip of the *F*-mode classical Cepheids becomes too narrow at low luminosity to allow for the occurrence of pulsators with period smaller than about one day.

[2] We deliberately ignore the possible presence of a magnetic field, which may make the interaction between rotation and pulsations even more complex.

Table 1. Results for the PW fitting for δ Sct variables.

α	β	γ	χ^2	n.Obj	Notes
0.764 ± 0.016	-4.444 ± 0.128		1.6 ± 0.1	6403	$-1.40 \leq \log_{10} P < -1.05$
0.730 ± 0.027	-2.921 ± 0.130		3.8 ± 0.6	2357	$-1.05 \leq \log_{10} P \leq -0.70$
0.796 ± 0.012	-3.773 ± 0.063	2.20 ± 0.21	2.3 ± 0.2	8760	$-1.40 \leq \log_{10} P \leq -0.70$

Notes. The fitted equations are $W = \alpha + \beta(\log_{10} P + \log_{10} P_0)$ or $W = \alpha + \beta(\log_{10} P + \log_{10} P_0) + \gamma(\log_{10} P + \log_{10} P_0)^2$, where we took $\log_{10} P_0 = 1.1$. The Notes column lists the period interval over which the different PW relations were calculated.

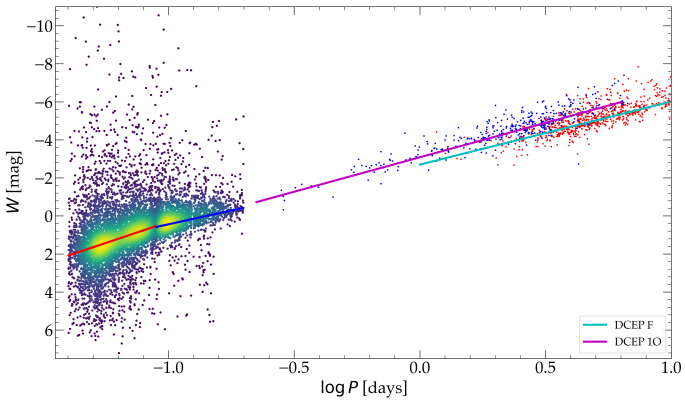


Fig. 13. Comparison between the PW relation(s) calculated in this paper for the fundamental F-mode δ Sct (as in Fig. 12) and those of F- (red dots) and the first overtone 1O-mode (blue dots) classical Cepheids. For the latter pulsators, the data and the PWs were taken from Poggio et al. (2021). For clarity, only objects with relative error on the photometric parallax better than 20% are plotted.

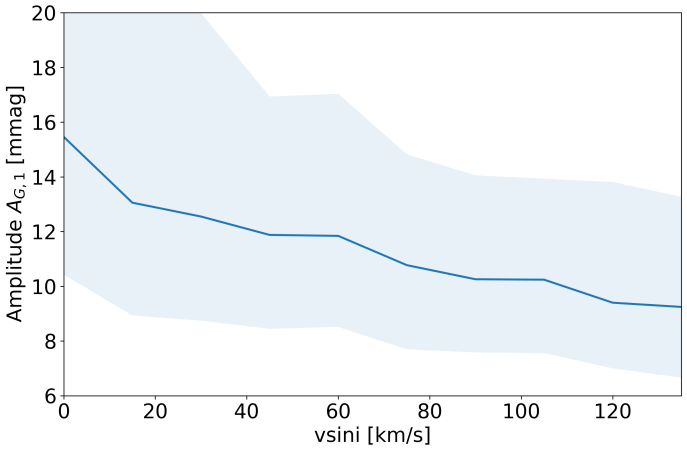


Fig. 14. Photometric amplitude A_1 in the *Gaia* G-band as a function of the $v \sin i$ derived from spectroscopic *Gaia* DR3 data for a sample of 3515 δ Sct stars. The dark blue line is the median amplitude for each $v \sin i$ bin of 15 km s^{-1} while the light blue band shows the 25%–75% quantile interval.

As expected, the bins are not equally populated. All bins contain at least 220 stars, except for the bin with the most rapid rotators for which the constraint on the $v \sin i$ precision resulted in only 29 stars. The result is shown in Fig. 14. The dark blue line denotes the median amplitude for each bin, and the light blue band shows the 25%–75% quantile interval of photometric amplitude $A_{G,1}$ in each bin. A clear and steady decline in median amplitude can be seen with increasing $v \sin i$ at a rate of roughly 46 µmag per km s^{-1}. We note that the sample of 3525 sources contains both HADS and normal δ Sct stars. The vast majority of HADS occur in the lowest $v \sin i$ bin, where they are responsible for the strong decrease in amplitude in that bin. The corresponding curve for normal δ Sct stars is far less pronounced in the low-$v \sin i$ bins, yet is clearly present in all $v \sin i$ bins. We cover δ Sct stars with slow to moderate rotation rates of $v \sin i < 150$ km s^{-1}. This is well below the $v \sin i = 270$ km s^{-1} of the fast-rotating δ Sct star Altair, whose dominant mode has an amplitude of only about 0.6 mmag in the white-light broad-band filter of the MOST space telescope (Le Dizès et al. 2021).

7. Summary and conclusions

In this paper, we present our investigation of the *Gaia* DR3 time series of stars classified as β Cep, SPB, γ Dor, or δ Sct by the CU7 classification pipeline. These stars are non-radial pulsators of intermediate and high mass and have proven to be excellent targets for asteroseismology (Aerts 2021; Kurtz 2023). They are often multi-periodic and have much lower amplitudes than RR Lyr stars or long-period variables. This makes them more challenging to detect and discriminate from other types of variables, in particular with the modest size and sparseness of a typical G-band time series in *Gaia* DR3. For this reason, we focused on time series with a least 40 data points.

Roughly half a million stars with at least 40 data points were classified in one of the four classes by the variability processing pipeline of CU7. Closer inspection of the results of the automated Fourier analysis of this pipeline showed that a variation of instrumental origin was detected for the majority of these stars. This points to imperfect calibrations of the photometric time series at mmag level. We expect these instrumental variations to be calibrated out in the *Gaia* DR5 release. We succeeded in filtering out most of the stars that show instrumental variations, at the cost of significantly reducing the sample size of IHM pulsators. Nevertheless, the approximately 106 K pulsators of this kind constitute an unseen sample in terms of size, magnitude range, and sky coverage. Our comparison with a subsample of the remaining stars in Sect. 4 shows that the main frequency ν_1 agrees very well with that found in the literature.

To assess the quality of our sample of IHM pulsators, we compared the position of the stars in the HR diagram with the theoretical instability strips. This requires the empirical $T_{\rm eff}$ and luminosity of each star, which we took from the *Gaia* DR3 `gspphot` data as derived by DPAC-CU8. We focused on the nearby stars with the most precise location in the HR diagram as observed by *Gaia*. For these stars, the empirical location of SPB, δ Sct, and γ Dor stars matched the theoretical instability strips quite well. We did find a fraction of ~20% pulsators to occur outside the strips, in between the SPB and δ Sct strip on the one hand, and below the γ Dor strip on the other. These pulsators have a dominant frequency expected for fast

rotators pulsating in gravito-inertial modes (Salmon et al. 2014; Saio et al. 2017; Aerts et al. 2019). For some of the β Cep stars, we noticed discrepant positions with respect to their strip. This may be caused by a systematic bias of the $T_{\rm eff}$ and/or the luminosity L as derived from `gspphot` data for the hottest stars. However, it may also suggest that the instability strips of OB-type stars are incompletely covered by the current physical descriptions of their interiors. The HR diagrams also revealed the presence of rotationally modulated stars. This is as expected since both ground-based data (e.g Briquet et al. 2007) and space photometry (Degroote et al. 2011; Balona 2016; Bowman et al. 2018; Balona et al. 2019, among others) already showed that rotationally modulated and pulsating stars co-exist inside the instability strips, and that the two populations of stars largely overlap.

Our analysis of the period–luminosity relation of δ Sct stars provides a good demonstration of the uniqueness of *Gaia* data, as *Gaia* DR3 is able to bring both ingredients to investigate this relation. To our knowledge, the empirical PW relation in Fig. 12 is the most extensive reported in the literature for δ Sct stars so far. We find evidence that the relation has two different regimes depending on the period of the dominant oscillation mode.

Finally, we are able to confirm that stellar rotation has a direct impact on the observed oscillation amplitude of δ Sct stars, in the sense that increasing rotation decreases the amplitude. The $v \sin i$ data necessary to establish this result were derived from *Gaia* DR3 spectroscopic `esphs` data. We were able to quantify the order of magnitude of the gradient, arriving at roughly 46 μmag per km s^{-1}.

Despite the not yet perfect photometric calibration of the *Gaia* DR3 data, we were able to demonstrate the great potential of combined and homogeneously sampled photometric, spectroscopic, and astrometric *Gaia* data to investigate OBAF-type main sequence pulsators, and we look forward to the more extensive *Gaia* DR4 and DR5 data for which we expect the time series to be less prone to high-frequency instrumental variations.

Acknowledgements. This work presents results from the European Space Agency (ESA) space mission *Gaia*. *Gaia* data are being processed by the *Gaia* Data Processing and Analysis Consortium (DPAC). Funding for the DPAC is provided by national institutions, in particular the institutions participating in the *Gaia* MultiLateral Agreement (MLA). The *Gaia* mission website is `https://www.cosmos.esa.int/gaia`. The *Gaia* archive website is `https://archives.esac.esa.int/gaia`. The full acknowledgements are available in Appendix A.

References

Aerts, C. 2021, Rev. Mod. Phys., 93, 015001
Aerts, C., Augustson, K., Mathis, S., et al. 2021, A&A, 656, A121
Aerts, C., & Kolenberg, K. 2005, A&A, 431, 615
Aerts, C., Molenberghs, G., Kenward, M. G., & Neiner, C. 2014, ApJ, 781, 88
Aerts, C., Molenberghs, G., Michielsen, M., et al. 2018, ApJS, 237, 15
Aerts, C., Mathis, S., & Rogers, T. M. 2019, ARA&A, 57, 35
Andrae, R., Fouesneau, M., Sordo, R., et al. 2023, A&A, 674, A27 (*Gaia* DR3 SI)
Antoci, V., Cunha, M. S., Bowman, D. M., et al. 2019, MNRAS, 490, 4040
Astropy Collaboration (Robitaille, T. P., et al.) 2013, A&A, 558, A33
Astropy Collaboration (Price-Whelan, A. M., et al.) 2018, AJ, 156, 123
Auvergne, M., Bodin, P., Boisnard, L., et al. 2009, A&A, 506, 411
Baade, D., Rivinius, T., Pigulski, A., et al. 2016, A&A, 588, A56
Baade, D., Pigulski, A., Rivinius, T., et al. 2018a, A&A, 610, A70
Baade, D., Pigulski, A., Rivinius, T., et al. 2018b, A&A, 620, A145
Bailer-Jones, C. A. L., Rybizki, J., Fouesneau, M., Demleitner, M., & Andrae, R. 2021, AJ, 161, 147
Balona, L. A. 2016, MNRAS, 457, 3724
Balona, L. A., & Ozuyar, D. 2020, MNRAS, 493, 5871
Balona, L. A., Ripepi, V., Catanzaro, G., et al. 2011a, MNRAS, 414, 792
Balona, L. A., Pigulski, A., De Cat, P., et al. 2011b, MNRAS, 413, 2403
Balona, L. A., Handler, G., Chowdhury, S., et al. 2019, MNRAS, 485, 3457
Baluev, R. V. 2008, MNRAS, 385, 1279
Bouchaud, K., Domiciano de Souza, A., Rieutord, M., Reese, D. R., & Kervella, P. 2020, A&A, 633, A78
Bowman, D. M., Kurtz, D. W., Breger, M., Murphy, S. J., & Holdsworth, D. L. 2016, MNRAS, 460, 1970
Bowman, D. M., Buysschaert, B., Neiner, C., et al. 2018, A&A, 616, A77
Breger, M. 1979, PASP, 91, 5
Breger, M. 1990, Delta Scuti Star Newsl., 2, 13
Breger, M. 2000, in Delta Scuti and Related Stars, eds. M. Breger, & M. Montgomery, ASP Conf. Ser., 210, 3
Briquet, M., Hubrig, S., De Cat, P., et al. 2007, A&A, 466, 269
Burssens, S., Simón-Díaz, S., Bowman, D. M., et al. 2020, A&A, 639, A81
Buysschaert, B., Aerts, C., Bowman, D. M., et al. 2018, A&A, 616, A148
Chen, X., Wang, S., Deng, L., et al. 2020, ApJS, 249, 18
Clementini, G., Ripepi, V., Molinaro, R., et al. 2019, A&A, 622, A60
Daszyńska-Daszkiewicz, J., Dziembowski, W. A., Pamyatnykh, A. A., & Goupil, M. J. 2002, A&A, 392, 151
Daszyńska-Daszkiewicz, J., Dziembowski, W. A., & Pamyatnykh, A. A. 2007, Acta Atron., 57, 11
Daszyńska-Daszkiewicz, J., Ostrowski, J., & Pamyatnykh, A. A. 2013, MNRAS, 432, 3153
Daszyńska-Daszkiewicz, J., Pamyatnykh, A. A., Walczak, P., et al. 2017, MNRAS, 466, 2284
Degroote, P., Aerts, C., Ollivier, M., et al. 2009, A&A, 506, 471
Degroote, P., Aerts, C., Baglin, A., et al. 2010, Nature, 464, 259
Degroote, P., Acke, B., Samadi, R., et al. 2011, A&A, 536, A82
Deng, Z. M., Li, Y., Wu, T., & Chen, X. H. 2018, Acta Astron. Sin., 59, 49
Dhouib, H., Prat, V., Van Reeth, T., & Mathis, S. 2021a, A&A, 652, A154
Dhouib, H., Prat, V., Van Reeth, T., & Mathis, S. 2021b, A&A, 656, A122
Diago, P. D., Gutiérrez-Soto, J., Auvergne, M., et al. 2009, A&A, 506, 125
Distefano, E., Lanzafame, A. C., Brugaletta, E., et al. 2023, A&A, 674, A20 (*Gaia* DR3 SI)
Drake, A. J., Djorgovski, S. G., Catelan, M., et al. 2017, MNRAS, 469, 3688
Dupret, M. A., Grigahcène, A., Garrido, R., Gabriel, M., & Scuflaire, R. 2005, A&A, 435, 927
Eker, Z., Soydugan, F., Bilir, S., et al. 2020, MNRAS, 496, 3887
Eyer, L., Audard, M., Holl, B., et al. 2023, A&A, 674, A13 (*Gaia* DR3 SI)
Gaia Collaboration (Prusti, T., et al.) 2016, A&A, 595, A1
Gaia Collaboration (Eyer, L., et al.) 2019, A&A, 623, A110
García, R. A., & Ballot, J. 2019, Liv. Rev. Sol. Phys., 16, 4
Gavras, P., Rimoldini, L., Nienartowicz, K., et al. 2023, A&A, 674, A22 (*Gaia* DR3 SI)
Gebruers, S., Straumit, I., Tkachenko, A., et al. 2021, A&A, 650, A151
Grigahcène, A., Antoci, V., Balona, L., et al. 2010, ApJ, 713, L192
Guzik, J. A., Kaye, A. B., Bradley, P. A., Cox, A. N., & Neuforge, C. 2000, ApJ, 542, L57
Harris, C. R., Millman, K. J., van der Walt, S. J., et al. 2020, Nature, 585, 357
Hekker, S., & Christensen-Dalsgaard, J. 2017, A&ARv, 25, 1
Henneco, J., Van Reeth, T., Prat, V., et al. 2021, A&A, 648, A97
Holl, B., Fabricius, C., Portell, J., et al. 2023, A&A, 674, A25 (*Gaia* DR3 SI)
Hon, M., Stello, D., & Yu, J. 2018, MNRAS, 476, 3233
Huat, A. L., Hubert, A. M., Baudin, F., et al. 2009, A&A, 506, 95
Hunter, J. D. 2007, Comput. Sci. Eng., 9, 90
Jayasinghe, T., Stanek, K. Z., Kochanek, C. S., et al. 2020, MNRAS, 493, 4186
Koch, D. G., Borucki, W. J., Basri, G., et al. 2010, ApJ, 713, L79
Kurtz, D. W. 2000, in Delta Scuti and Related Stars, eds. M. Breger, & M. Montgomery, ASP Conf. Ser., 210, 287
Kurtz, D. 2023, ARA&A, in press, [arXiv:2201.11629]
Kurtz, D. W., Saio, H., Takata, M., et al. 2014, MNRAS, 444, 102
Labadie-Bartz, J., Baade, D., Carciofi, A. C., et al. 2021, MNRAS, 502, 242
Le Dizès, C., Rieutord, M., & Charpinet, S. 2021, A&A, 653, A26
Lee, U. 2021, MNRAS, 505, 1495
Lee, U., & Saio, H. 2020, MNRAS, 497, 4117
Li, G., Van Reeth, T., Bedding, T. R., et al. 2020, MNRAS, 491, 3586
Lindegren, L., Bastian, U., Biermann, M., et al. 2021, A&A, 649, A4
McKinney, W. 2010, in Proceedings of the 9th Python in Science Conference, eds. S. van der Walt, & J. Millman, 56
McNamara, D. H. 2011, AJ, 142, 110
McNamara, D. H., Clementini, G., & Marconi, M. 2007, AJ, 133, 2752
Miglio, A., Montalbán, J., & Dupret, M.-A. 2007, MNRAS, 375, L21
Mombarg, J. S. G., Van Reeth, T., Pedersen, M. G., et al. 2019, MNRAS, 485, 3248
Mombarg, J. S. G., Dotter, A., Van Reeth, T., et al. 2020, ApJ, 895, 51
Mombarg, J. S. G., Van Reeth, T., & Aerts, C. 2021, A&A, 650, A58
Moravveji, E., Aerts, C., Pápics, P. I., Triana, S. A., & Vandoren, B. 2015, A&A, 580, A27
Mowlavi, N., Barblan, F., Saesen, S., & Eyer, L. 2013, A&A, 554, A108
Mowlavi, N., Saesen, S., Semaan, T., et al. 2016, A&A, 595, L1

Mowlavi, N., Lecoeur-Taïbi, I., Lebzelter, T., et al. 2018, A&A, 618, A58
Moździerski, D., Pigulski, A., Kopacki, G., Kołaczkowski, Z., & Stęślicki, M. 2014, Acta Atron., 64, 89
Moździerski, D., Pigulski, A., Kołaczkowski, Z., et al. 2019, A&A, 632, A95
Murphy, S. J., Fossati, L., Bedding, T. R., et al. 2016, MNRAS, 459, 1201
Murphy, S. J., Hey, D., Van Reeth, T., & Bedding, T. R. 2019, MNRAS, 485, 2380
Neiner, C., Gutiérrez-Soto, J., Baudin, F., et al. 2009, A&A, 506, 143
Neiner, C., Floquet, M., Samadi, R., et al. 2012, A&A, 546, A47
Ouazzani, R. M., Lignières, F., Dupret, M. A., et al. 2020, A&A, 640, A49
Palaversa, L., Ivezić, Ž., Eyer, L., et al. 2013, AJ, 146, 101
Pamyatnykh, A. A. 1999, Acta Atron., 49, 119
Pápics, P. I., Briquet, M., Baglin, A., et al. 2012, A&A, 542, A55
Pápics, P. I., Tkachenko, A., Van Reeth, T., et al. 2017, A&A, 598, A74
Pedersen, M. G., Chowdhury, S., Johnston, C., et al. 2019, ApJ, 872, L9
Pedersen, M. G., Escorza, A., Pápics, P. I., & Aerts, C. 2020, MNRAS, 495, 2738
Pedersen, M. G., Aerts, C., Pápics, P. I., et al. 2021, Nat. Astron., 5, 715
Pérez, F., & Granger, B. E. 2007, Comput. Sci. Eng., 9, 21
Pigulski, A., & Pojmański, G. 2009, in Stellar Pulsation: Challenges for Theory and Observation, eds. J. A. Guzik, & P. A. Bradley, Am. Inst. Phys. Conf. Ser., 1170, 351
Poggio, E., Drimmel, R., Cantat-Gaudin, T., et al. 2021, A&A, 651, A104
Poro, A., Paki, E., Mazhari, G., et al. 2021, PASP, 133, 084201
Reese, D. R., Prat, V., Barban, C., van 't Veer-Menneret, C., & MacGregor, K. B. 2013, A&A, 550, A77
Reese, D. R., Mirouh, G. M., Espinosa Lara, F., Rieutord, M., & Putigny, B. 2021, A&A, 645, A46
Ricker, G. R., Vanderspek, R., Winn, J., et al. 2016, in Space Telescopes and Instrumentation 2016: Optical, Infrared, and Millimeter Wave, eds. H. A. MacEwen, G. G. Fazio, M. Lystrup, et al., SPIE Conf. Ser., 9904, 99042B
Riess, A. G., Casertano, S., Yuan, W., et al. 2021, ApJ, 908, L6
Rimoldini, L., & Holl, B. 2022, Gaia DR3 documentation Chapter 10: Variability, Gaia DR3 documentation
Rimoldini, L., Holl, B., Gavras, P., et al. 2023, A&A, 674, A14 (*Gaia* DR3 SI)
Ripepi, V., Catanzaro, G., Clementini, G., et al. 2022, A&A, 659, A167
Rivinius, T., Baade, D., & Štefl, S. 2003, A&A, 411, 229
Rivinius, T., Carciofi, A. C., & Martayan, C. 2013, A&ARv, 21, 69
Rodríguez, E., & López-González, M. J. 2000, A&A, 359, 597
Rodríguez, E., López-González, M. J., & López de Coca, P. 2000, A&AS, 144, 469
Rybizki, J., Green, G. M., Rix, H.-W., et al. 2022, MNRAS, 510, 2597
Saesen, S., Carrier, F., Pigulski, A., et al. 2010, A&A, 515, A16
Saesen, S., Briquet, M., Aerts, C., Miglio, A., & Carrier, F. 2013, AJ, 146, 102
Saio, H., Kurtz, D. W., Takata, M., et al. 2015, MNRAS, 447, 3264
Saio, H., Ekström, S., Mowlavi, N., et al. 2017, MNRAS, 467, 3864
Saio, H., Bedding, T. R., Kurtz, D. W., et al. 2018, MNRAS, 477, 2183
Salmon, S. J. A. J., Montalbán, J., Reese, D. R., Dupret, M. A., & Eggenberger, P. 2014, A&A, 569, A18
Schmid, V. S., & Aerts, C. 2016, A&A, 592, A116
Sekaran, S., Tkachenko, A., Johnston, C., & Aerts, C. 2021, A&A, 648, A91
Sharma, A. N., Bedding, T. R., Saio, H., & White, T. R. 2022, MNRAS, 515, 828
Smith, M. A., & Henry, G. W. 2021, ApJ, 915, 13
Stankov, A., & Handler, G. 2005, ApJS, 158, 193
Stello, D., Saunders, N., Grunblatt, S., et al. 2022, MNRAS, 512, 1677
Struve, O. 1955, PASP, 67, 135
Szewczuk, W., & Daszyńska-Daszkiewicz, J. 2017, MNRAS, 469, 13
Szewczuk, W., & Daszyńska-Daszkiewicz, J. 2018, MNRAS, 478, 2243
Szewczuk, W., Walczak, P., & Daszyńska-Daszkiewicz, J. 2021, MNRAS, 503, 5894
Taylor, M. B. 2005, in Astronomical Data Analysis Software and Systems XIV, eds. P. Shopbell, M. Britton, & R. Ebert, ASP Conf. Ser., 347, 29
Townsend, R. H. D. 2005, MNRAS, 364, 573
Van Beeck, J., Bowman, D. M., Pedersen, M. G., et al. 2021, A&A, 655, A59
Van Reeth, T., Tkachenko, A., Aerts, C., et al. 2015, ApJS, 218, 27
Van Reeth, T., Tkachenko, A., & Aerts, C. 2016, A&A, 593, A120
Van Reeth, T., Mombarg, J. S. G., Mathis, S., et al. 2018, A&A, 618, A24
Virtanen, P., Gommers, R., Oliphant, T. E., et al. 2020, Nat. Methods, 17, 261
White, T. R., Pope, B. J. S., Antoci, V., et al. 2017, MNRAS, 471, 2882
Wu, T., Li, Y., Deng, Z.-M., et al. 2020, ApJ, 899, 38
Xiong, D. R., Deng, L., Zhang, C., & Wang, K. 2016, MNRAS, 457, 3163
Yu, J., Huber, D., Bedding, T. R., et al. 2018, ApJS, 236, 42
Yu, J., Bedding, T. R., Stello, D., et al. 2020, MNRAS, 493, 1388
Yu, J., Hekker, S., Bedding, T. R., et al. 2021, MNRAS, 501, 5135
Zechmeister, M., & Kürster, M. 2009, A&A, 496, 577
Ziaali, E., Bedding, T. R., Murphy, S. J., Van Reeth, T., & Hey, D. R. 2019, MNRAS, 486, 4348

[1] Instituut voor Sterrenkunde, KU Leuven, Celestijnenlaan 200D, 3001 Leuven, Belgium
[2] INAF – Osservatorio Astronomico di Capodimonte, Via Moiariello 16, 80131 Napoli, Italy
[3] Department of Astrophysics/IMAPP, Radboud University, PO Box 9010, 6500 GL Nijmegen, The Netherlands
[4] Max Planck Institute for Astronomy, Königstuhl 17, 69117 Heidelberg, Germany
[5] Ruđer Bošković Institute, Bijenička cesta 54, 10000 Zagreb, Croatia
[6] Institute of Astronomy, University of Cambridge, Madingley Road, Cambridge CB3 0HA, UK
[7] Department of Astronomy, University of Geneva, Chemin Pegasi 51, 1290 Versoix, Switzerland
[8] Department of Astronomy, University of Geneva, Chemin d'Ecogia 16, 1290 Versoix, Switzerland
[9] Leiden Observatory, Leiden University, Niels Bohrweg 2, 2333 CA Leiden, The Netherlands
[10] INAF – Osservatorio astronomico di Padova, Vicolo Osservatorio 5, 35122 Padova, Italy
[11] European Space Agency (ESA), European Space Research and Technology Centre (ESTEC), Keplerlaan 1, 2201 AZ Noordwijk, The Netherlands
[12] GEPI, Observatoire de Paris, Université PSL, CNRS, 5 Place Jules Janssen, 92190 Meudon, France
[13] Univ. Grenoble Alpes, CNRS, IPAG, 38000 Grenoble, France
[14] Astronomisches Rechen-Institut, Zentrum für Astronomieder Universität Heidelberg, Mönchhofstr. 12-14, 69120 Heidelberg, Germany
[15] Université Côte d'Azur, Observatoire de la Côte d'Azur, CNRS, Laboratoire Lagrange, Bd de l'Observatoire, CS 34229, 06304 Nice Cedex 4, France
[16] Laboratoire d'astrophysique de Bordeaux, Univ. Bordeaux, CNRS, B18N, allée Geoffroy Saint-Hilaire, 33615 Pessac, France
[17] European Space Agency (ESA), European Space Astronomy Centre (ESAC), Camino bajo del Castillo, s/n, Urbanizacion Villafranca del Castillo, Villanueva de la Cañada, 28692 Madrid, Spain
[18] Aurora Technology for European Space Agency (ESA), Camino bajo del Castillo, s/n, Urbanizacion Villafranca del Castillo, Villanueva de la Cañada, 28692 Madrid, Spain
[19] Institut de Ciències del Cosmos (ICCUB), Universitat de Barcelona (IEEC-UB), Martí i Franquès 1, 08028 Barcelona, Spain
[20] Lohrmann Observatory, Technische Universität Dresden, Mommsenstraße 13, 01062 Dresden, Germany
[21] Lund Observatory, Department of Astronomy and Theoretical Physics, Lund University, Box 43, 22100 Lund, Sweden
[22] CNES Centre Spatial de Toulouse, 18 avenue Edouard Belin, 31401 Toulouse Cedex 9, France
[23] Institut d'Astronomie et d'Astrophysique, Université Libre de Bruxelles CP 226, Boulevard du Triomphe, 1050 Brussels, Belgium
[24] F.R.S.-FNRS, Rue d'Egmont 5, 1000 Brussels, Belgium
[25] INAF – Osservatorio Astrofisico di Arcetri, Largo Enrico Fermi 5, 50125 Firenze, Italy
[26] INAF – Osservatorio Astrofisico di Torino, via Osservatorio 20, 10025 Pino Torinese (TO), Italy
[27] European Space Agency (ESA), Noordwijk, The Netherlands
[28] University of Turin, Department of Physics, Via Pietro Giuria 1, 10125 Torino, Italy
[29] INAF – Osservatorio di Astrofisica e Scienza dello Spazio di Bologna, via Piero Gobetti 93/3, 40129 Bologna, Italy
[30] DAPCOM for Institut de Ciències del Cosmos (ICCUB), Universitat de Barcelona (IEEC-UB), Martí i Franquès 1, 08028 Barcelona, Spain
[31] Royal Observatory of Belgium, Ringlaan 3, 1180 Brussels, Belgium

[32] Observational Astrophysics, Division of Astronomy and Space Physics, Department of Physics and Astronomy, Uppsala University, Box 516, 751 20 Uppsala, Sweden
[33] ALTEC S.p.a, Corso Marche, 79, 10146 Torino, Italy
[34] Sednai Sàrl, Geneva, Switzerland
[35] Mullard Space Science Laboratory, University College London, Holmbury St Mary, Dorking, Surrey RH5 6NT, UK
[36] Gaia DPAC Project Office, ESAC, Camino bajo del Castillo, s/n, Urbanizacion Villafranca del Castillo, Villanueva de la Cañada, 28692 Madrid, Spain
[37] Telespazio UK S.L. for European Space Agency (ESA), Camino bajo del Castillo, s/n, Urbanizacion Villafranca del Castillo, Villanueva de la Cañada, 28692 Madrid, Spain
[38] SYRTE, Observatoire de Paris, Université PSL, CNRS, Sorbonne Université, LNE, 61 avenue de l'Observatoire, 75014 Paris, France
[39] National Observatory of Athens, I. Metaxa and Vas. Pavlou, Palaia Penteli, 15236 Athens, Greece
[40] IMCCE, Observatoire de Paris, Université PSL, CNRS, Sorbonne Université, Univ. Lille, 77 av. Denfert-Rochereau, 75014 Paris, France
[41] Serco Gestión de Negocios for European Space Agency (ESA), Camino bajo del Castillo, s/n, Urbanizacion Villafranca del Castillo, Villanueva de la Cañada, 28692 Madrid, Spain
[42] Institut d'Astrophysique et de Géophysique, Université de Liège, 19c, Allée du 6 Août, 4000 Liège, Belgium
[43] CRAAG – Centre de Recherche en Astronomie, Astrophysique et Géophysique, Route de l'Observatoire Bp 63 Bouzareah, 16340 Algiers, Algeria
[44] Institute for Astronomy, University of Edinburgh, Royal Observatory, Blackford Hill, Edinburgh EH9 3HJ, UK
[45] RHEA for European Space Agency (ESA), Camino bajo del Castillo, s/n, Urbanizacion Villafranca del Castillo, Villanueva de la Cañada, 28692 Madrid, Spain
[46] ATG Europe for European Space Agency (ESA), Camino bajo del Castillo, s/n, Urbanizacion Villafranca del Castillo, Villanueva de la Cañada, 28692 Madrid, Spain
[47] CIGUS CITIC – Department of Computer Science and Information Technologies, University of A Coruña, Campus de Elviña s/n, A Coruña 15071, Spain
[48] Université de Strasbourg, CNRS, Observatoire astronomique de Strasbourg, UMR 7550, 11 rue de l'Université, 67000 Strasbourg, France
[49] Kavli Institute for Cosmology Cambridge, Institute of Astronomy, Madingley Road, Cambridge CB3 0HA, UK
[50] Leibniz Institute for Astrophysics Potsdam (AIP), An der Sternwarte 16, 14482 Potsdam, Germany
[51] CENTRA, Faculdade de Ciências, Universidade de Lisboa, Edif. C8, Campo Grande, 1749-016 Lisboa, Portugal
[52] Department of Informatics, Donald Bren School of Information and Computer Sciences, University of California, Irvine, 5226 Donald Bren Hall, 92697-3440, CA Irvine, USA
[53] INAF – Osservatorio Astrofisico di Catania, via S. Sofia 78, 95123 Catania, Italy
[54] Dipartimento di Fisica e Astronomia "Ettore Majorana", Università di Catania, Via S. Sofia 64, 95123 Catania, Italy
[55] INAF – Osservatorio Astronomico di Roma, Via Frascati 33, 00078 Monte Porzio Catone (Roma), Italy
[56] Space Science Data Center – ASI, Via del Politecnico SNC, 00133 Roma, Italy
[57] Department of Physics, University of Helsinki, PO Box 64, 00014 Helsinki, Finland
[58] Finnish Geospatial Research Institute FGI, Geodeetinrinne 2, 02430 Masala, Finland
[59] Institut UTINAM CNRS UMR6213, Université Bourgogne Franche-Comté, OSU THETA Franche-Comté Bourgogne, Observatoire de Besançon, BP1615, 25010 Besançon Cedex, France
[60] HE Space Operations BV for European Space Agency (ESA), Keplerlaan 1, 2201 AZ Noordwijk, The Netherlands
[61] Dpto. de Inteligencia Artificial, UNED, c/Juan del Rosal 16, 28040 Madrid, Spain
[62] Konkoly Observatory, Research Centre for Astronomy and Earth Sciences, Eötvös Loránd Research Network (ELKH), MTA Centre of Excellence, Konkoly Thege Miklós út 15-17, 1121 Budapest, Hungary
[63] ELTE Eötvös Loránd University, Institute of Physics, 1117, Pázmány Péter sétány 1A, Budapest, Hungary
[64] University of Vienna, Department of Astrophysics, Türkenschanzstraße 17, A1180 Vienna, Austria
[65] Institute of Physics, Laboratory of Astrophysics, Ecole Polytechnique Fédérale de Lausanne (EPFL), Observatoire de Sauverny, 1290 Versoix, Switzerland
[66] Kapteyn Astronomical Institute, University of Groningen, Landleven 12, 9747 AD Groningen, The Netherlands
[67] School of Physics and Astronomy/Space Park Leicester, University of Leicester, University Road, Leicester LE1 7RH, UK
[68] Thales Services for CNES Centre Spatial de Toulouse, 18 avenue Edouard Belin, 31401 Toulouse Cedex 9, France
[69] Depto. Estadística e Investigación Operativa. Universidad de Cádiz, Avda. República Saharaui s/n, 11510 Puerto Real, Cádiz, Spain
[70] Center for Research and Exploration in Space Science and Technology, University of Maryland Baltimore County, 1000 Hilltop Circle, Baltimore, MD, USA
[71] GSFC – Goddard Space Flight Center, Code 698, 8800 Greenbelt Rd, 20771, MD Greenbelt, USA
[72] EURIX S.r.l., Corso Vittorio Emanuele II 61, 10128 Torino, Italy
[73] Porter School of the Environment and Earth Sciences, Tel Aviv University, Tel Aviv 6997801, Israel
[74] Harvard-Smithsonian Center for Astrophysics, 60 Garden St., MS 15, Cambridge, MA 02138, USA
[75] HE Space Operations BV for European Space Agency (ESA), Camino bajo del Castillo, s/n, Urbanizacion Villafranca del Castillo, Villanueva de la Cañada, 28692 Madrid, Spain
[76] Instituto de Astrofísica e Ciências do Espaço, Universidade do Porto, CAUP, Rua das Estrelas, 4150-762 Porto, Portugal
[77] LFCA/DAS, Universidad de Chile, CNRS, Casilla 36-D, Santiago, Chile
[78] SISSA – Scuola Internazionale Superiore di Studi Avanzati, via Bonomea 265, 34136 Trieste, Italy
[79] Telespazio for CNES Centre Spatial de Toulouse, 18 avenue Edouard Belin, 31401 Toulouse Cedex 9, France
[80] University of Turin, Department of Computer Sciences, Corso Svizzera 185, 10149 Torino, Italy
[81] Dpto. de Matemática Aplicada y Ciencias de la Computación, Univ. de Cantabria, ETS Ingenieros de Caminos, Canales y Puertos, Avda. de los Castros s/n, 39005 Santander, Spain
[82] Centro de Astronomía – CITEVA, Universidad de Antofagasta, Avenida Angamos 601, Antofagasta 1270300, Chile
[83] DLR Gesellschaft für Raumfahrtanwendungen (GfR) mbH, Münchener Straße 20, 82234 Weßling, Germany
[84] Centre for Astrophysics Research, University of Hertfordshire, College Lane, 10 9AB Hatfield, UK
[85] University of Turin, Mathematical Department "G. Peano", Via Carlo Alberto 10, 10123 Torino, Italy
[86] INAF – Osservatorio Astronomico d'Abruzzo, Via Mentore Maggini, 64100 Teramo, Italy
[87] Instituto de Astronomia, Geofisica e Ciências Atmosféricas, Universidade de São Paulo, Rua do Matão, 1226, Cidade Universitaria, 05508-900 São Paulo, SP, Brazil
[88] APAVE SUDEUROPE SAS for CNES Centre Spatial de Toulouse, 18 avenue Edouard Belin, 31401 Toulouse Cedex 9, France
[89] Mésocentre de calcul de Franche-Comté, Université de Franche-Comté, 16 route de Gray, 25030 Besançon Cedex, France
[90] ATOS for CNES Centre Spatial de Toulouse, 18 avenue Edouard Belin, 31401 Toulouse Cedex 9, France
[91] School of Physics and Astronomy, Tel Aviv University, Tel Aviv 6997801, Israel
[92] Astrophysics Research Centre, School of Mathematics and Physics, Queen's University Belfast, Belfast BT7 1NN, UK
[93] Centre de Données Astronomique de Strasbourg, Strasbourg, France

[94] Institute for Computational Cosmology, Department of Physics, Durham University, Durham DH1 3LE, UK
[95] European Southern Observatory, Karl-Schwarzschild-Str. 2, 85748 Garching, Germany
[96] Max-Planck-Institut für Astrophysik, Karl-Schwarzschild-Straße 1, 85748 Garching, Germany
[97] Data Science and Big Data Lab, Pablo de Olavide University, 41013 Seville, Spain
[98] Barcelona Supercomputing Center (BSC), Plaça Eusebi Güell 1-3, 08034 Barcelona, Spain
[99] ETSE Telecomunicación, Universidade de Vigo, Campus Lagoas-Marcosende, 36310 Vigo, Galicia, Spain
[100] Asteroid Engineering Laboratory, Space Systems, Luleå University of Technology, Box 848, S-981 28 Kiruna, Sweden
[101] Vera C Rubin Observatory, 950 N. Cherry Avenue, Tucson, AZ 85719, USA
[102] Department of Astrophysics, Astronomy and Mechanics, National and Kapodistrian University of Athens, Panepistimiopolis, Zografos, 15783 Athens, Greece
[103] TRUMPF Photonic Components GmbH, Lise-Meitner-Straße 13, 89081 Ulm, Germany
[104] IAC – Instituto de Astrofisica de Canarias, Via Láctea s/n, 38200 La Laguna S.C., Tenerife, Spain
[105] Department of Astrophysics, University of La Laguna, Via Láctea s/n, 38200 La Laguna S.C., Tenerife, Spain
[106] Faculty of Aerospace Engineering, Delft University of Technology, Kluyverweg 1, 2629 Simon Vestdijkpad 24, 2321 WD HS Delft, The Netherlands
[107] Radagast Solutions, Simon Vestdijkpad 24, 2321, WD Leiden, The Netherlands
[108] Laboratoire Univers et Particules de Montpellier, CNRS Université Montpellier, Place Eugène Bataillon, CC72, 34095 Montpellier Cedex 05, France
[109] Université de Caen Normandie, Côte de Nacre Boulevard Maréchal Juin, 14032 Caen, France
[110] LESIA, Observatoire de Paris, Université PSL, CNRS, Sorbonne Université, Université de Paris, 5 Place Jules Janssen, 92190 Meudon, France
[111] SRON Netherlands Institute for Space Research, Niels Bohrweg 4, 2333 CA Leiden, The Netherlands
[112] Astronomical Observatory, University of Warsaw, Al. Ujazdowskie 4, 00-478 Warszawa, Poland
[113] Scalian for CNES Centre Spatial de Toulouse, 18 avenue Edouard Belin, 31401 Toulouse Cedex 9, France
[114] Université Rennes, CNRS, IPR (Institut de Physique de Rennes) – UMR 6251, 35000 Rennes, France
[115] Shanghai Astronomical Observatory, Chinese Academy of Sciences, 80 Nandan Road, Shanghai 200030, PR China
[116] University of Chinese Academy of Sciences, No. 19(A) Yuquan Road, Shijingshan District, Beijing 100049, PR China
[117] Niels Bohr Institute, University of Copenhagen, Juliane Maries Vej 30, 2100 Copenhagen Ø, Denmark
[118] DXC Technology, Retortvej 8, 2500 Valby, Denmark
[119] Las Cumbres Observatory, 6740 Cortona Drive Suite 102, Goleta, CA 93117, USA
[120] CIGUS CITIC, Department of Nautical Sciences and Marine Engineering, University of A Coruña, Paseo de Ronda 51, 15071 A Coruña, Spain
[121] Astrophysics Research Institute, Liverpool John Moores University, 146 Brownlow Hill, Liverpool L3 5RF, UK
[122] IPAC, Mail Code 100-22, California Institute of Technology, 1200 E. California Blvd., Pasadena, CA 91125, USA
[123] IRAP, Université de Toulouse, CNRS, UPS, CNES, 9 Av. colonel Roche, BP 44346, 31028 Toulouse Cedex 4, France
[124] MTA CSFK Lendület Near-Field Cosmology Research Group, Konkoly Observatory, MTA Research Centre for Astronomy and Earth Sciences, Konkoly Thege Miklós út 15-17, 1121 Budapest, Hungary
[125] Departmento de Física de la Tierra y Astrofísica, Universidad Complutense de Madrid, 28040 Madrid, Spain
[126] Villanova University, Department of Astrophysics and Planetary Science, 800 E Lancaster Avenue, Villanova, PA 19085, USA
[127] INAF – Osservatorio Astronomico di Brera, via E. Bianchi, 46, 23807 Merate (LC), Italy
[128] STFC, Rutherford Appleton Laboratory, Harwell, Didcot OX11 0QX, UK
[129] Charles University, Faculty of Mathematics and Physics, Astronomical Institute of Charles University, V Holesovickach 2, 18000 Prague, Czech Republic
[130] Department of Particle Physics and Astrophysics, Weizmann Institute of Science, Rehovot 7610001, Israel
[131] Department of Astrophysical Sciences, 4 Ivy Lane, Princeton University, Princeton, NJ 08544, USA
[132] Departamento de Astrofísica, Centro de Astrobiología (CSIC-INTA), ESA-ESAC. Camino Bajo del Castillo s/n., 28692 Villanueva de la Cañada, Madrid, Spain
[133] naXys, University of Namur, Rempart de la Vierge, 5000 Namur, Belgium
[134] CGI Deutschland B.V. & Co. KG, Mornewegstr. 30, 64293 Darmstadt, Germany
[135] Institute of Global Health, University of Geneva, Geneva, Switzerland
[136] Astronomical Observatory Institute, Faculty of Physics, Adam Mickiewicz University, Poznań, Poland
[137] H H Wills Physics Laboratory, University of Bristol, Tyndall Avenue, Bristol BS8 1TL, UK
[138] Department of Physics and Astronomy G. Galilei, University of Padova, Vicolo dell'Osservatorio 3, 35122 Padova, Italy
[139] CERN, Esplanade des Particules 1, PO Box 1211, Geneva, Switzerland
[140] Applied Physics Department, Universidade de Vigo, 36310 Vigo, Spain
[141] Association of Universities for Research in Astronomy, 1331 Pennsylvania Ave. NW, Washington, DC 20004, USA
[142] European Southern Observatory, Alonso de Córdova 3107, Casilla 19, Santiago, Chile
[143] Sorbonne Université, CNRS, UMR7095, Institut d'Astrophysique de Paris, 98bis bd. Arago, 75014 Paris, France
[144] Faculty of Mathematics and Physics, University of Ljubljana, Jadranska ulica 19, 1000 Ljubljana, Slovenia

Appendix A: Acknowledgements

The *Gaia* mission and data processing have financially been supported by, in alphabetical order by country:

- the Algerian Centre de Recherche en Astronomie, Astrophysique et Géophysique of Bouzareah Observatory;
- the Austrian Fonds zur Förderung der wissenschaftlichen Forschung (FWF) Hertha Firnberg Programme through grants T359, P20046, and P23737;
- the BELgian federal Science Policy Office (BELSPO) through various PROgramme de Développement d'Expériences scientifiques (PRODEX) grants, and the Research Foundation Flanders (Fonds Wetenschappelijk Onderzoek) through grant VS.091.16N, and the Fonds de la Recherche Scientifique (FNRS), and the Research Council of Katholieke Universiteit (KU) Leuven through grant C16/18/005 (Pushing AsteRoseismology to the next level with TESS, GaiA, and the Sloan DIgital Sky SurvEy – PARADISE);
- the Brazil-France exchange programmes Fundação de Amparo à Pesquisa do Estado de São Paulo (FAPESP) and Coordenação de Aperfeicoamento de Pessoal de Nível Superior (CAPES) - Comité Français d'Evaluation de la Coopération Universitaire et Scientifique avec le Brésil (COFECUB);
- the Chilean Agencia Nacional de Investigación y Desarrollo (ANID) through Fondo Nacional de Desarrollo Científico y Tecnológico (FONDECYT) Regular Project 1210992 (L. Chemin);
- the National Natural Science Foundation of China (NSFC) through grants 11573054, 11703065, and 12173069, the China Scholarship Council through grant 201806040200, and the Natural Science Foundation of Shanghai through grant 21ZR1474100;
- the Tenure Track Pilot Programme of the Croatian Science Foundation and the École Polytechnique Fédérale de Lausanne and the project TTP-2018-07-1171 'Mining the Variable Sky', with the funds of the Croatian-Swiss Research Programme;
- the Czech-Republic Ministry of Education, Youth, and Sports through grant LG 15010 and INTER-EXCELLENCE grant LTAUSA18093, and the Czech Space Office through ESA PECS contract 98058;
- the Danish Ministry of Science;
- the Estonian Ministry of Education and Research through grant IUT40-1;
- the European Commission's Sixth Framework Programme through the European Leadership in Space Astrometry (ELSA) Marie Curie Research Training Network (MRTN-CT-2006-033481), through Marie Curie project PIOF-GA-2009-255267 (Space AsteroSeismology & RR Lyrae stars, SAS-RRL), and through a Marie Curie Transfer-of-Knowledge (ToK) fellowship (MTKD-CT-2004-014188); the European Commission's Seventh Framework Programme through grant FP7-606740 (FP7-SPACE-2013-1) for the *Gaia* European Network for Improved data User Services (GENIUS) and through grant 264895 for the *Gaia* Research for European Astronomy Training (GREAT-ITN) network;
- the European Cooperation in Science and Technology (COST) through COST Action CA18104 'Revealing the Milky Way with *Gaia*(MW-Gaia)';
- the European Research Council (ERC) through grants 320360, 647208, and 834148 and through the European Union's Horizon 2020 research and innovation and excellent science programmes through Marie Skłodowska-Curie grant 745617 (Our Galaxy at full HD – Gal-HD) and 895174 (The build-up and fate of self-gravitating systems in the Universe) as well as grants 687378 (Small Bodies: Near and Far), 682115 (Using the Magellanic Clouds to Understand the Interaction of Galaxies), 695099 (A sub-percent distance scale from binaries and Cepheids – CepBin), 716155 (Structured ACCREtion Disks – SACCRED), 951549 (Sub-percent calibration of the extragalactic distance scale in the era of big surveys – UniverScale), and 101004214 (Innovative Scientific Data Exploration and Exploitation Applications for Space Sciences – EXPLORE);
- the European Science Foundation (ESF), in the framework of the *Gaia* Research for European Astronomy Training Research Network Programme (GREAT-ESF);
- the European Space Agency (ESA) in the framework of the *Gaia* project, through the Plan for European Cooperating States (PECS) programme through contracts C98090 and 4000106398/12/NL/KML for Hungary, through contract 4000115263/15/NL/IB for Germany, and through PROgramme de Développement d'Expériences scientifiques (PRODEX) grant 4000127986 for Slovenia;
- the Academy of Finland through grants 299543, 307157, 325805, 328654, 336546, and 345115 and the Magnus Ehrnrooth Foundation;
- the French Centre National d'Études Spatiales (CNES), the Agence Nationale de la Recherche (ANR) through grant ANR-10-IDEX-0001-02 for the 'Investissements d'avenir' programme, through grant ANR-15-CE31-0007 for project 'Modelling the Milky Way in the *Gaia*era' (MOD4Gaia), through grant ANR-14-CE33-0014-01 for project 'The Milky Way disc formation in the *Gaia*era' (ARCHEOGAL), through grant ANR-15-CE31-0012-01 for project 'Unlocking the potential of Cepheids as primary distance calibrators' (UnlockCepheids), through grant ANR-19-CE31-0017 for project 'Secular evolution of galxies' (SEGAL), and through grant ANR-18-CE31-0006 for project 'Galactic Dark Matter' (GaDaMa), the Centre National de la Recherche Scientifique (CNRS) and its SNO *Gaia*of the Institut des Sciences de l'Univers (INSU), its Programmes Nationaux: Cosmologie et Galaxies (PNCG), Gravitation Références Astronomie Métrologie (PNGRAM), Planétologie (PNP), Physique et Chimie du Milieu Interstellaire (PCMI), and Physique Stellaire (PNPS), the 'Action Fédératrice *Gaia*' of the Observatoire de Paris, the Région de Franche-Comté, the Institut National Polytechnique (INP) and the Institut National de Physique nucléaire et de Physique des Particules (IN2P3) co-funded by CNES;
- the German Aerospace Agency (Deutsches Zentrum für Luft- und Raumfahrt e.V., DLR) through grants 50QG0501, 50QG0601, 50QG0602, 50QG0701, 50QG0901, 50QG 1001, 50QG1101, 50QG1401, 50QG1402, 50QG1403, 50QG1404, 50QG1904, 50QG2101, 50QG2102, and 50QG2202, and the Centre for Information Services and High Performance Computing (ZIH) at the Technische Universität Dresden for generous allocations of computer time;
- the Hungarian Academy of Sciences through the Lendület Programme grants LP2014-17 and LP2018-7 and the Hungarian National Research, Development, and Innovation Office (NKFIH) through grant KKP-137523 ('SeismoLab');
- the Science Foundation Ireland (SFI) through a Royal Society - SFI University Research Fellowship (M. Fraser);

– the Israel Ministry of Science and Technology through grant 3-18143 and the Tel Aviv University Center for Artificial Intelligence and Data Science (TAD) through a grant;
– the Agenzia Spaziale Italiana (ASI) through contracts I/037/08/0, I/058/10/0, 2014-025-R.0, 2014-025-R.1.2015, and 2018-24-HH.0 to the Italian Istituto Nazionale di Astrofisica (INAF), contract 2014-049-R.0/1/2 to INAF for the Space Science Data Centre (SSDC, formerly known as the ASI Science Data Center, ASDC), contracts I/008/10/0, 2013/030/I.0, 2013-030-I.0.1-2015, and 2016-17-I.0 to the Aerospace Logistics Technology Engineering Company (ALTEC S.p.A.), INAF, and the Italian Ministry of Education, University, and Research (Ministero dell'Istruzione, dell'Università e della Ricerca) through the Premiale project 'MIning The Cosmos Big Data and Innovative Italian Technology for Frontier Astrophysics and Cosmology' (MITiC);
– the Netherlands Organisation for Scientific Research (NWO) through grant NWO-M-614.061.414, through a VICI grant (A. Helmi), and through a Spinoza prize (A. Helmi), and the Netherlands Research School for Astronomy (NOVA);
– the Polish National Science Centre through HARMONIA grant 2018/30/M/ST9/00311 and DAINA grant 2017/27/L/ST9/03221 and the Ministry of Science and Higher Education (MNiSW) through grant DIR/WK/2018/12;
– the Portuguese Fundação para a Ciência e a Tecnologia (FCT) through national funds, grants SFRH/BD/128840/2017 and PTDC/FIS-AST/30389/2017, and work contract DL 57/2016/CP1364/CT0006, the Fundo Europeu de Desenvolvimento Regional (FEDER) through grant POCI-01-0145-FEDER-030389 and its Programa Operacional Competitividade e Internacionalização (COMPETE2020) through grants UIDB/04434/2020 and UIDP/04434/2020, and the Strategic Programme UIDB/00099/2020 for the Centro de Astrofísica e Gravitação (CENTRA);
– the Slovenian Research Agency through grant P1-0188;
– the Spanish Ministry of Economy (MINECO/FEDER, UE), the Spanish Ministry of Science and Innovation (MICIN), the Spanish Ministry of Education, Culture, and Sports, and the Spanish Government through grants BES-2016-078499, BES-2017-083126, BES-C-2017-0085, ESP2016-80079-C2-1-R, ESP2016-80079-C2-2-R, FPU16/03827, PDC2021-121059-C22, RTI2018-095076-B-C22, and TIN2015-65316-P ('Computación de Altas Prestaciones VII'), the Juan de la Cierva Incorporación Programme (FJCI-2015-2671 and IJC2019-04862-I for F. Anders), the Severo Ochoa Centre of Excellence Programme (SEV2015-0493), and MICIN/AEI/10.13039/501100011033 (and the European Union through European Regional Development Fund 'A way of making Europe') through grant RTI2018-095076-B-C21, the Institute of Cosmos Sciences University of Barcelona (ICCUB, Unidad de Excelencia 'María de Maeztu') through grant CEX2019-000918-M, the University of Barcelona's official doctoral programme for the development of an R+D+i project through an Ajuts de Personal Investigador en Formació (APIF) grant, the Spanish Virtual Observatory through project AyA2017-84089, the Galician Regional Government, Xunta de Galicia, through grants ED431B-2021/36, ED481A-2019/155, and ED481A-2021/296, the Centro de Investigación en Tecnologías de la Información y las Comunicaciones (CITIC), funded by the Xunta de Galicia and the European Union (European Regional Development Fund – Galicia 2014-2020 Programme), through grant ED431G-2019/01, the Red Española de Supercomputación (RES) computer resources at MareNostrum, the Barcelona Supercomputing Centre - Centro Nacional de Supercomputación (BSC-CNS) through activities AECT-2017-2-0002, AECT-2017-3-0006, AECT-2018-1-0017, AECT-2018-2-0013, AECT-2018-3-0011, AECT-2019-1-0010, AECT-2019-2-0014, AECT-2019-3-0003, AECT-2020-1-0004, and DATA-2020-1-0010, the Departament d'Innovació, Universitats i Empresa de la Generalitat de Catalunya through grant 2014-SGR-1051 for project 'Models de Programació i Entorns d'Execució Parallels' (MPEXPAR), and Ramon y Cajal Fellowship RYC2018-025968-I funded by MICIN/AEI/10.13039/501100011033 and the European Science Foundation ('Investing in your future');
– the Swedish National Space Agency (SNSA/Rymdstyrelsen);
– the Swiss State Secretariat for Education, Research, and Innovation through the Swiss Activités Nationales Complémentaires and the Swiss National Science Foundation through an Eccellenza Professorial Fellowship (award PCEFP2_194638 for R. Anderson);
– the United Kingdom Particle Physics and Astronomy Research Council (PPARC), the United Kingdom Science and Technology Facilities Council (STFC), and the United Kingdom Space Agency (UKSA) through the following grants to the University of Bristol, the University of Cambridge, the University of Edinburgh, the University of Leicester, the Mullard Space Sciences Laboratory of University College London, and the United Kingdom Rutherford Appleton Laboratory (RAL): PP/D006511/1, PP/D006546/1, PP/D006570/1, ST/I000852/1, ST/J005045/1, ST/K00056X/1, ST/K000209/1, ST/K000756/1, ST/L006561/1, ST/N000595/1, ST/N000641/1, ST/N000978/1, ST/N001117/1, ST/S000089/1, ST/S000976/1, ST/S000984/1, ST/S001123/1, ST/S001948/1, ST/S001980/1, ST/S002103/1, ST/V000969/1, ST/W002469/1, ST/W002493/1, ST/W002671/1, ST/W002809/1, and EP/V520342/1.

The GBOT programme uses observations collected at (i) the European Organisation for Astronomical Research in the Southern Hemisphere (ESO) with the VLT Survey Telescope (VST), under ESO programmes 092.B-0165, 093.B-0236, 094.B-0181, 095.B-0046, 096.B-0162, 097.B-0304, 098.B-0030, 099.B-0034, 0100.B-0131, 0101.B-0156, 0102.B-0174, and 0103.B-0165; and (ii) the Liverpool Telescope, which is operated on the island of La Palma by Liverpool John Moores University in the Spanish Observatorio del Roque de los Muchachos of the Instituto de Astrofísica de Canarias with financial support from the United Kingdom Science and Technology Facilities Council, and (iii) telescopes of the Las Cumbres Observatory Global Telescope Network.

In addition we thank Dr. Eric Gosset as well as the anonymous referee for useful comments.

For an up-to-date list of acknowledgements, contributors, and former contributors to the *Gaia*project, we refer to the following URL: https://gea.esac.esa.int/archive/documentation/GDR3/Miscellaneous/sec_acknowl/

This work made use of Python (Python Software Foundation) and the IPython software (Pérez & Granger 2007), as well as of the Python packages Numpy (Harris et al. 2020), Pandas (McKinney 2010), Matplotlib (Hunter 2007), Astropy (Astropy Collaboration 2013, 2018). In addition we made use of the visualisation software TOPCAT (Taylor 2005), and the

National Aeronautics and Space Administration (NASA) Astrophysics Data System (ADS).

Appendix B: Gaia DR3 data of asteroseismically modelled *Kepler* γ Dor and SPB stars

We extracted the *Gaia* DR3 time series in the Gaia *G*-band for 63 well-known bona fide g-mode pulsators assembled in Aerts et al. (2021). This sample consists of 37 γ Dor and 26 SPB pulsators whose internal structure and evolutionary stage have been modelled asteroseismically using *Kepler* photometric time series that were reduced by Van Reeth et al. (2015) and Pedersen et al. (2021). The *Kepler* light curves typically have a total time base of $\sim$ 1470 d and between some 24 000 and 66 000 data points, with an even sampling time of $\sim$ 30 minutes (Koch et al. 2010). The *Gaia* DR3 epoch photometric data of these g-mode pulsators is sparsely sampled, containing between 34 and 52 data points spread over a time base of between about 910 and 920 d. We re-analysed these *Kepler* light curves in the Fourier domain in the same way as was done for the *Gaia* DR3 *G*-band epoch photometry, using the generalised Lomb-Scargle periodogram (Zechmeister & Kürster 2009), and extracted the two dominant frequencies in the interval $[0, 25]\,\mathrm{d}^{-1}$. After derivation of the dominant periodic signal, the second strongest frequency was extracted after prewhitening of the dominant frequency and its harmonics up to fourth order.

Given that the *Kepler* data are almost free of any aliasing, while instrumental effects occur at the level of only a few μmag, we know the two dominant frequencies of these 63 g-mode pulsating dwarfs up to high precision. This allows us to assess the occurrence of the instrumental effects present in the Gaia DR3 G-band epoch photometry, which occur at mmag level and hence contaminate the pulsational g-mode signal quite severely. Figure B.1 shows a histogram with the 63 pulsators according to their dominant g-mode frequency deduced from the *Kepler* data (in blue). The dominant frequency in the Gaia data is indicated by the black hatched histogram and reveals that most of the detected dominant frequencies occur above $6\,\mathrm{d}^{-1}$ indicating that they are either aliased frequencies or frequencies of instrumental origin.

The passband of the *Kepler* CCDs is somewhat bluer and narrower than the Gaia *G*-band. Moreover, the 63 g-mode pulsators each reveal tens of g modes with accompanying multi-periodic beating in time (Van Reeth et al. 2015; Pedersen et al. 2021). The amplitude of the dominant signal in the *Kepler* and Gaia *G*-band are therefore not expected to be equal. Nevertheless, they are of the same order, and so it is meaningful to consider their distributions. This is revealed in Fig. B.2, which shows the dominant frequencies detected in the 126 light curves, in grey for the Gaia DR3 G-band data and in colour for the *Kepler* data (pink for the 37 γ Dor stars and blue for the 26 SPB stars). It can be seen that the majority of the mode frequencies occurs in the range $[0.2, 3.1]\,\mathrm{d}^{-1}$, as is well known for gravito-inertial modes in rotating stars (Aerts et al. 2021). The dominant modes of these 63 well-known g-mode pulsators have amplitudes covering the range [0.5, 33] mmag, with the majority well below 10 mmag. While several of the dominant frequencies detected in the Gaia G-band occur in the appropriate frequency range, Figure B.2 clearly shows the presence of peaks at high frequencies, which are either aliased frequencies or periodic instrumental artefacts.

Close inspection of Fig. B.2 reveals that 6 of the 37 γ Dor stars (16%) and 4 of the 26 SPB stars (15%) share the same dominant intrinsic g-mode frequency in their *Kepler* and Gaia G-band data. This is illustrated for the γ Dor star KIC 11080103 in Fig. B.3 and for the SPB KIC 4936089 in Fig. B.4. KIC 11080103 has a dominant prograde dipole mode with frequency $1.241393\,\mathrm{d}^{-1}$ and amplitude of 12.13 mmag in the *Kepler* band (Van Reeth et al. 2015). The SPB star KIC 4936089, whose periodograms are shown in Fig. B.4, has a dominant g-mode frequency of $0.866263\,\mathrm{d}^{-1}$ with an amplitude of 6.26 mmag. Its *Kepler* light curve revealed a period spacing pattern consisting of 13 zonal dipole modes of consecutive radial order. This SPB star ranks number 8 of 26 in terms of dominant mode amplitude, yet the 52 Gaia *G*data points do allow to pick up the dominant mode, thanks to relatively modest instrumental contamination for this star (Fig. B.4). These two examples show that the amplitude of the dominant frequency peak in the

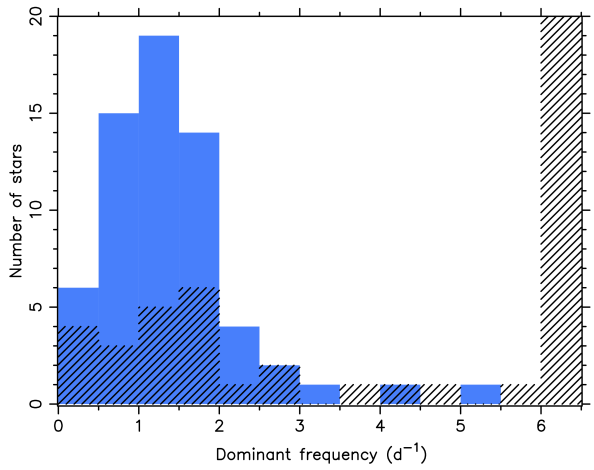


Fig. B.1. Histogram of the dominant frequency in the *Kepler* light curves of 63 asteroseismically modelled g-mode pulsators (blue) compared with the dominant frequency occurring in their Gaia DR3 G-band epoch photometry (black hatched). For reasons of visibility, the $x-$axis is cut at $6.5\,\mathrm{d}^{-1}$ and the $y-$axis at 20; 38 of the 63 g-mode pulsators have their Gaia data dominated by instrumental effects with dominant frequency above $6\,\mathrm{d}^{-1}$ rather than by their g modes.

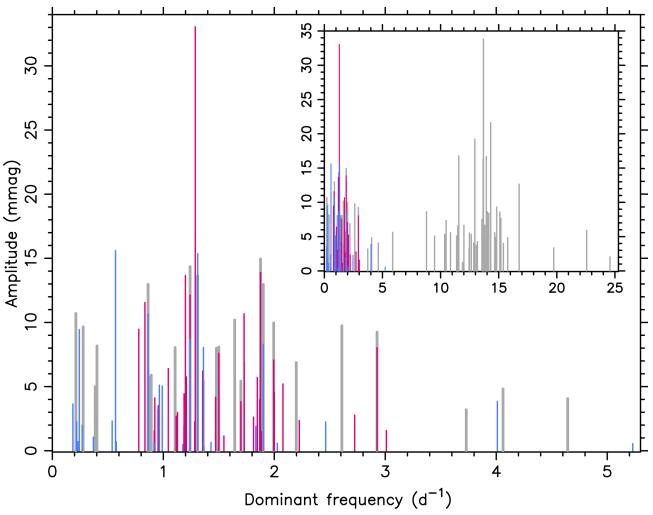


Fig. B.2. Amplitudes of the dominant frequencies in the Gaia G-band DR3 light curves (grey) and in the *Kepler* light curves of the γ Dor (pink) and SPB (blue) pulsators. The inset shows the entire frequency range, while the main panel focuses on the range of the true dominant g-mode frequencies of the 63 stars.

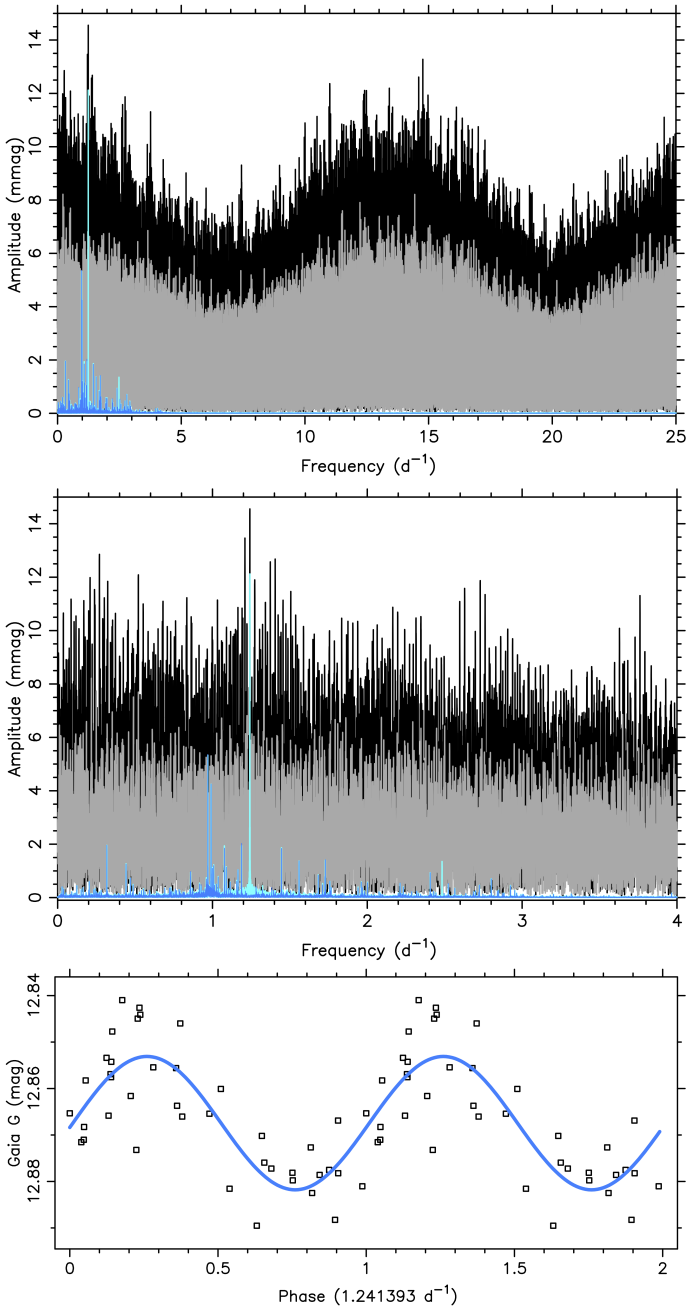


Fig. B.3. Four Lomb-Scargle periodograms (upper: full frequency range; middle; zoomed version) of the γ Dor star KIC 11080103. The black and cyan curves stand for the Gaia DR3 G-band and *Kepler* light curves, respectively. The grey and blue periodograms result from prewhitening the Gaia G and *Kepler* data with the dominant frequency. The lower panel shows the Gaia DR3 G-band data (black squares) folded with the dominant frequency detected in common in both light curves; a harmonic fit with that frequency is overplotted (full blue line). For visibility purposes, the phase is shown for two cycles.

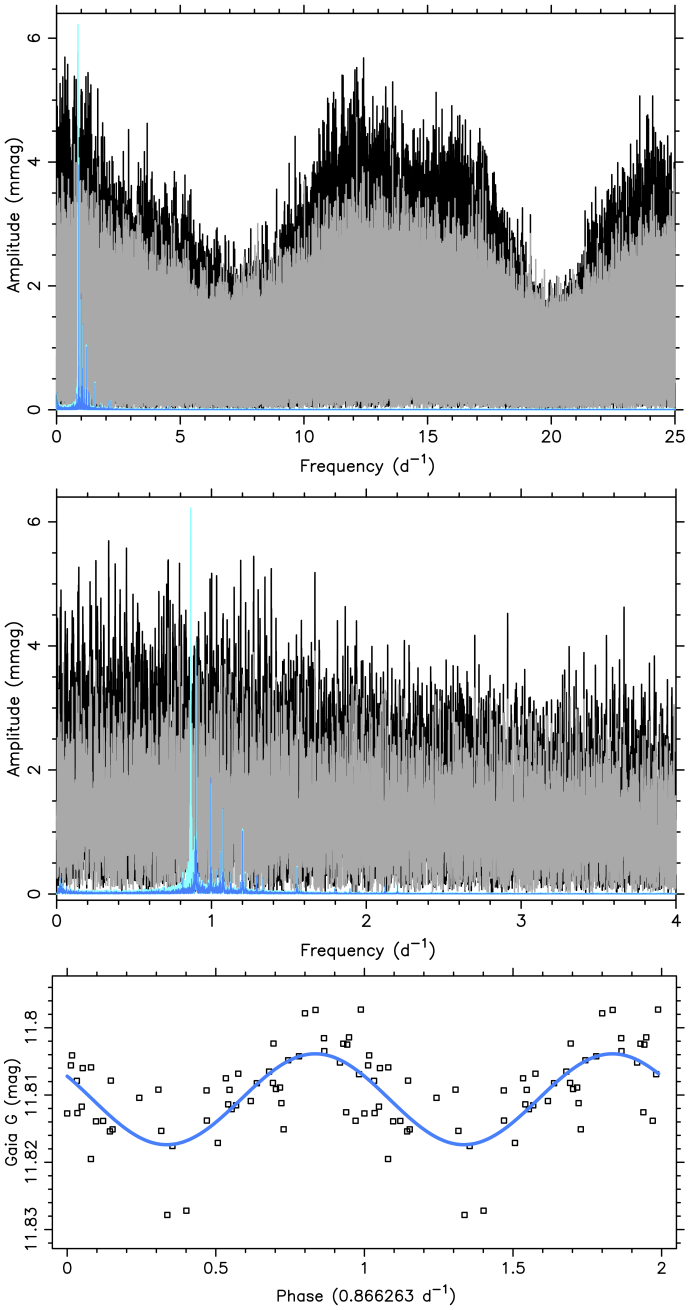


Fig. B.4. Same as Fig. B.3, but for the SPB star KIC 4936089.

periodogram is not a good criterion to select g-mode pulsators (compare the upper panels of Figs B.3 and B.4).

KIC 11080103 and KIC 4936089 are representative for six of the other cases where *Kepler* and Gaia G-band data lead to the same dominant frequency, with similar morphologies in the periodograms as those shown in Figs B.3 and B.4. It concerns the four γ Dor stars KIC 3448365, KIC 7365537, KIC 7434470, KIC 9480469, with dominant g-mode frequencies of 1.500150 d^{-1}, 2.925633 d^{-1}, 1.698729 d^{-1}, 1.994846 d^{-1}, respectively, and the two SPB stars KIC 5941844 and KIC 9020774 with dominant frequencies of 1.309558 d^{-1} and 1.900723 d^{-1}.

For one single γ Dor star, KIC 7023122, and one single SPB star, KIC 7760680, also the second strongest frequencies coincide in the *Kepler* and Gaia G data. The four phase diagrams of these two 'best cases' among the g-mode pulsators are shown in Figs B.5 and B.6. These two examples show that, despite the limited number of measurements in the DR3 time series, Gaia's G-band data already allow us to detect multiperiodic non-radial oscillations at mmag level, albeit it for a very small fraction (3%) of pulsating dwarfs pulsators.

We also checked for all 63 stars if it is meaningful to use the fraction of the variance in the data explained by a harmonic fit

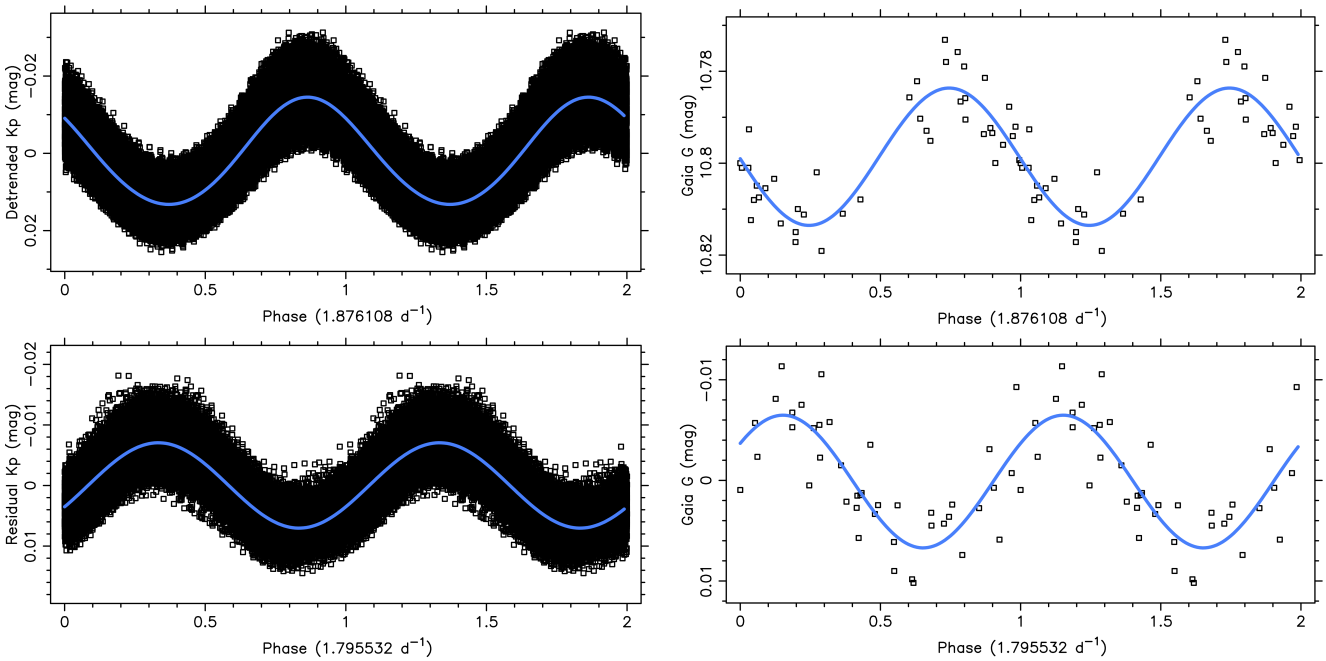


Fig. B.5. Four phase diagrams for the γ Dor pulsator KIC 7023122 whose two dominant g-mode frequencies (as listed in the legend of the $x-$axes) occur consistently in the periodograms of the Gaia DR3 G-band and *Kepler* photometry. The data are shown as black squares and the best harmonic fits for the fixed frequencies as blue lines. For visibility purposes, the phases are shown for two cycles.

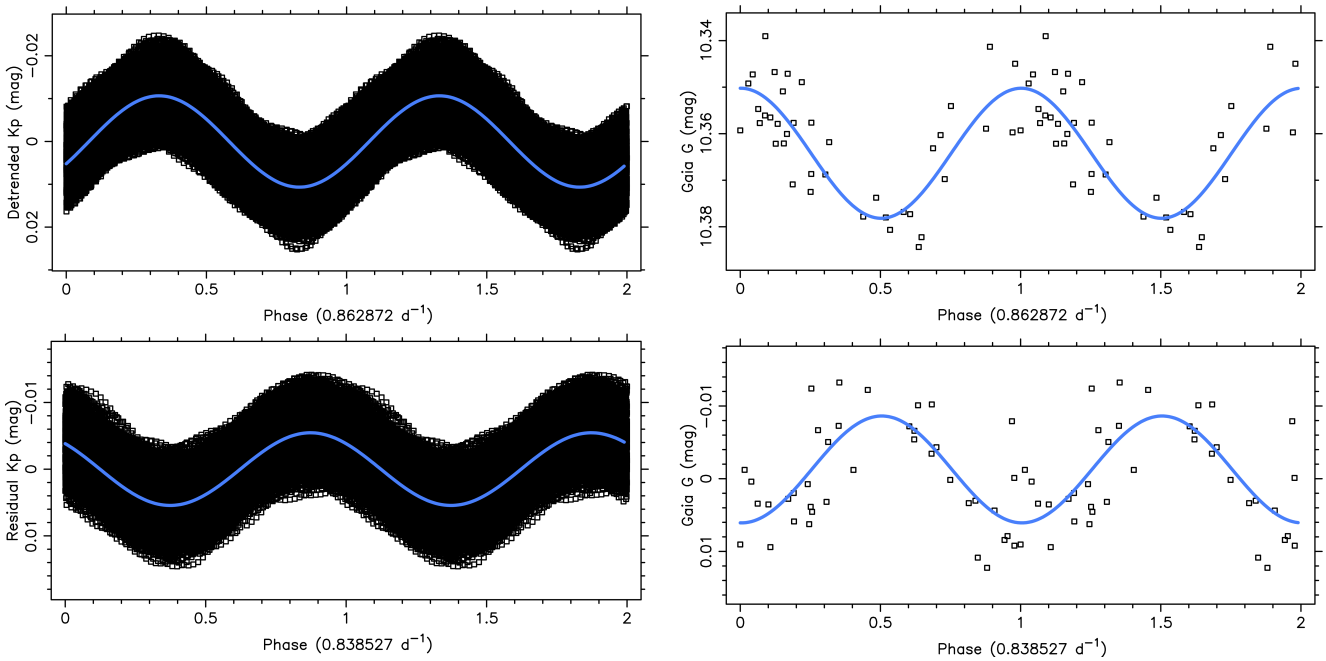


Fig. B.6. Same as Fig. B.5 but for the SPB star KIC 7760680.

with the dominant frequency as a selection criterion to distinguish intrinsic g-mode frequencies from instrumental frequencies. We found this not to be feasible, as this merit function attains similar values for instrumental and intrinsic frequencies. The corresponding phase diagrams also do not allow to distinguish between intrinsic and aliased/instrumental frequencies in a meaningful way. This is illustrated in Fig. B.7 for the largest-amplitude γ Dor pulsator of the sample. Figure B.7 shows two phase diagrams based on the 40 Gaia DR3 G-band data points: one based on the 'true' intrinsic dominant g-mode frequency reducing the variance by 47% and another one using the dominant frequency in the data themselves, which is either aliased or of instrumental origin. The latter frequency reduces the variance by 58%. Hence the variance reduction cannot be used as a criterion to distinguish between instrumental and true frequencies in *Gaia*'s DR3 time series.

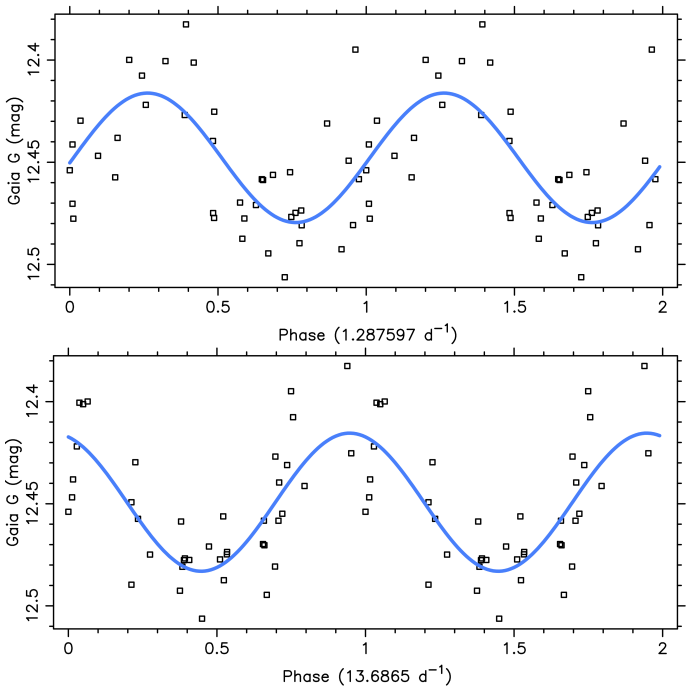


Fig. B.7. Two phase diagrams for the largest-amplitude g-mode pulsator in the γ Dor sample. The upper graph is phase-folded with the true dominant g-mode frequency derived from *Kepler* data; its fit leads to a variance reduction in the Gaia DR3 G-band data of 47%. The lower graph is phase-folded with the dominant frequency in the data, which is of instrumental origin and reduces the variance with 58%.